BRNO UNIVERSITY OF TECHNOLOGY
VYSOKÉ UČENÍ TECHNICKÉ V BRNĚ

FACULTY OF CHEMISTRY
FAKULTA CHEMICKÁ

INSTITUTE OF MATERIALS SCIENCE
ÚSTAV CHEMIE MATERIÁLŮ

ENCAPSULATION OF GROWTH FACTORS USING LIPOSOMES
ENKAPSULACE RŮSTOVÝCH FAKTORŮ POMOCÍ LIPOSOMŮ

MASTER'S THESIS
DIPLOMOVÁ PRÁCE

AUTHOR — **Bc. Zuzana Kadlecová**
AUTOR PRÁCE

SUPERVISOR — **Ing. Jana Brtníková, Ph.D.**
VEDOUCÍ PRÁCE

BRNO 2021

VYSOKÉ UČENÍ TECHNICKÉ V BRNĚ
FAKULTA CHEMICKÁ

Zadání diplomové práce

Číslo práce:	FCH-DIP1602/2020	Akademický rok:	2020/21
Ústav:	Ústav chemie materiálů		
Studentka:	**Bc. Zuzana Kadlecová**		
Studijní program:	Chemie, technologie a vlastnosti materiálů		
Studijní obor:	Chemie, technologie a vlastnosti materiálů		
Vedoucí práce:	**Ing. Jana Brtníková, Ph.D.**		

Název diplomové práce:

Enkapsulace růstových faktorů pomocí liposomů

Zadání diplomové práce:

1) Literární rešerše na téma stabilizace proteinů pomocí liposomů.
2) Příprava liposomů.
3)Charakterizace a sledování fyzikálních a chemických vlastností připravených enkasulovaných proteinů.
4) Vyhodnocení výsledků a jejich diskuse.
5) Závěr.

Termín odevzdání diplomové práce: 30.7.2021:

Diplomová práce se odevzdává v děkanem stanoveném počtu exemplářů na sekretariát ústavu. Toto zadání je součástí diplomové práce.

Bc. Zuzana Kadlecová student(ka)	Ing. Jana Brtníková, Ph.D. vedoucí práce	doc. Ing. František Šoukal, Ph.D. vedoucí ústavu

V Brně dne 1.2.2021

prof. Ing. Martin Weiter, Ph.D.
děkan

Abstract

The presented diploma thesis is focused on the current state of pro-healing fibroblast growth factor-2 (FGF2) stabilization via liposomes. FGF2 in its "wild" form is stable only for short periods of time due to its hydrolytical degradation that happens easily and leads to loss of its activity and efficacy. FGF2 is used in hard and soft tissue regeneration, for example, in healing of various skin injuries, chronical wounds, burns, or opened wounds related to type 1 and type 2 diabetes.

The aim of this thesis was to encapsulate hyper-stabilized FGF2 (FGF2-STAB®) of which *in vitro* activity is prolonged by its mutation from original 10 hours to up to 20 days at 37 °C. Nevertheless, based on our experiments, we discovered that this protein tends to bind to a polymeric or composite matrix from which it is slowly released, but its activity might change in time. Moreover, its activity decreases fast *in vivo* due to its diffusion through tissues and due to enzymatic degradation. To prolong its half-life, prevent undesirable interaction with the matrix, and to decrease the risk of degradation in *in vivo* applications, encapsulation of FGF2-STAB® into liposomes was considered. Liposomes represent a noninvasive way for transdermal drug delivery. They help the encapsulated drug to penetrate into the deeper layers of the skin thanks to its small diameter in the range of nanometres, which is advantageous in the relatively big molecule of FGF2-STAB® (22.5 kDa). Liposomes provide an additional protective layer to the encapsulated drug, which is then less prone to oxidation and degradation with changes in temperature or pH, but also its shelf life can be prolonged.

Theoretical part of the thesis brings an introduction to transdermal drug delivery problematic, presenting a brief introduction into liposomes, their types, stability, and liposomal drug delivery is discussed. A structure, origin, and use of fibroblast growth factor-2 are mentioned. In the experimental part, liposomes based on phosphatidylcholine (PC) and cholesterol were prepared using the reverse phase evaporation method. Stability via zeta potential, particle size and particle size distribution via dynamic light scattering (DLS) and scanning transmission electron microscopy (STEM) were observed in the prepared liposomes. Encapsulation efficiency was determined in liposomes containing FGF2-STAB® using ultraviolet-visible (UV-VIS) spectrophotometer in the presence of Bradford reagent. For liposome reparation optimization and for future comparison with FGF2-STAB® loaded liposomes, liposomes containing only phosphate buffer saline were prepared first. Different PC to cholesterol and PC to FGF2-STAB® ratios were tested. The best results were obtained using a 1,000:1 PC to FGF2-STAB® ratio according to the observed variables. Stability of liposomes to pH via zeta potential was observed and the parameters were optimized. Liposomes with effectively encapsulated FGF2-STAB® with a particle diameter around 100 nm have a great potential in systems with controlled drug release, such as composite scaffolds for bone and skin regeneration, in hydrogels for internal and topical wound healing applications as well as in cosmetics.

Keywords

Drug delivery systems, fibroblast growth factor-2, FGF2-STAB®, encapsulation efficiency, zeta potential.

Abstrakt

Předložená diplomová práce je zaměřena na současnou problematiku stabilizace pro-hojivého fibroblastového růstového faktoru-2 (FGF2) pomocí lipozomů. FGF2 je ve své „divoké“ formě stabilní pouze krátkodobě vzhledem k tomu, že snadno podléhá hydrolytické degradaci, čímž ztrácí svoji aktivitu a účinnost. Využívá se například při regeneraci tvrdých i měkkých tkání, např. při léčbě různých kožních poranění, chronických ran, popálenin nebo otevřených ran spojených s onemocněním diabetu prvního a druhého typu.

Cílem této práce bylo enkapsulovat hyperstabilizovaný FGF2 (FGF2-STAB®) jehož aktivita *in vitro* je mutacemi prodloužena z původních 10 hodin až na 20 dní při 37 °C. Nicméně, na základě námi provedených experimentů jsme zjistili, že se tento protein váže na polymerní či kompozitní matrice, ze kterých se pomalu uvolňuje s tím, že se jeho aktivita může časem měnit. Navíc, jeho aktivita rychle klesá *in vivo* v důsledku difúze tkáněmi a enzymatické degradace. Aby se prodloužil jeho poločas rozpadu, zabránilo se nežádoucím interakcím s matricí a snížilo se riziko degradace v aplikacích *in vivo*, zabývali jsme se stabilizací FGF2-STAB® jeho enkapsulací do lipozomů. Lipozomy představují neinvazivní způsob pro transdermální aplikaci léčiv. Napomáhají enkapsulované látce snáze pronikat do hlubších vrstev kůže, a to díky jejich malé velikosti v řádu nanometrů, což je u docela velké molekuly FGF2-STAB® (22,5 kDa) výhodné. Kromě toho poskytují dodatečnou ochrannou vrstvu, a látka je tak méně náchylná k oxidaci a degradaci vlivem změny pH či teploty. Navíc se také zvyšuje její celková doba skladovatelnosti a použitelnosti.

V teoretické části je zpracován úvod do problematiky aplikace léčiv transdermální cestou, stručný úvod do liposomů, jsou uvedeny typy lipozomů, jejich stabilita a princip uvolňování léčiva z lipozomů. Dále je zmíněna struktura, původ a využití fibroblastového růstového faktoru-2. V experimentální části byly metodou odpařování reverzní fáze připraveny lipozomy na bázi fosfatidylcholinu (PC) a cholesterolu. U připravených lipozomů byla vždy sledována stabilita částic pomocí zeta potenciálu, jejich velikost a distribuce velikosti těchto částic pomocí dynamického rozptylu světla (DLS) a rastrovací transmisní elektronové (STEM) analýzy. U lipozomů obsahujících FGF2-STAB® byla také vyhodnocena enkapsulační efektivita za pomocí ultrafialovo-viditelného (UV-VIS) spektrofotometru v přítomnosti Bradfordova činidla. Pro optimalizaci metody přípravy lipozomů a pro možnost srovnávání s lipozomy plněnými FGF2-STAB®, byly nejprve připraveny lipozomy plněné pouze fosfátovým pufrem. Byly testovány rozdílné poměry PC a cholesterolu a také rozdílné poměry PC a FGF2-STAB®. Nejlepších výsledků bylo dosaženo poměrem 1 000:1 PC k FGF2-STAB® vzhledem ke stanovovaným parametrům. Následně byla sledována stabilita lipozomů v závislosti na pH pomocí zeta potenciálu a jednotlivé parametry byly optimalizovány. Lipozomy s efektivně zaenkapsulovaným FGF2-STAB® s velikostí částic kolem 100 nm mají vysoký potenciál pro aplikace v systémech s postupným uvolňováním léčiva, jako jsou např. kompozitní nosiče pro regeneraci kostí i kůže nebo v hydrogelech pro vnitřní i topické aplikace hojení ran či v kosmetických přípravcích.

Klíčová slova

Nosiče pro dodávání léčiv, fibroblastový růstový faktor-2, FGF2-STAB®, enkapsulační efektivita, zeta potenciál.

KADLECOVÁ, Zuzana. *Encapsulation of growth factors into liposomes.* Brno, 2021. Brno University of Technology, Faculty of Chemistry, 2021. 59 p. Supervisor Ing. Jana Brtníková, Ph.D.

Declaration

I declare that the master thesis has been worked out by myself and that all the quotations from the literary sources are accurate and complete. The content of the diploma thesis is the property of the Faculty of Chemistry of Brno University of Technology, and all commercial uses are allowed only if approved by both the supervisor and the dean of the Faculty of Chemistry, BUT.

In Brno **28. 7 2021** ……

student's signature

Acknowledgements

I would like to thank to my supervisor Ing. Jana Brtníková, Ph.D. for the valuable advice, kindliness, and the time she has given me during my work on the thesis. I also want to thank doc. Ing. Lucy Vojtová, Ph.D., Ing. Klára Lysáková and Ing. Lenka Michlovská, Ph.D. for their willingness and patience in often consultations and guidance in the laboratory. Last but not least, I would like to thank Ing. Jana Dorazilová for help with STEM imaging and evaluation. CzechNanoLab project LM2018110 funded by MEYS CR is gratefully acknowledged for the financial support of the measurements/sample fabrication at CEITEC Nano Research Infrastructure.

I would also like to thank my family and close friends for their support during my studies and their tolerance of me being a try-hard.

CONTENT

1 INTRODUCTION

Transdermal delivery of drugs, therapeutic agents, and biologically active substances is an appealing method for many reasons – there is less enzymatic activity on the skin when compared to other administration methods and it dodges first-pass degradation in the liver [1]. However, when a drug is applied to the skin, the delivery is limited by the staggering properties of the skin and the transdermal delivery efficiency is not ideal. Therefore, various strategies have been researched to improve the penetration of a drug into the deeper layers of the skin. Physical technologies (i.e., sonophoresis, iontophoresis) use different types of energy to achieve disruption of the skin, while some invasive techniques (i.e., microneedles) disrupt the skin barrier to allow direct access to the epidermis [1, 2].

This thesis is focused on specific non-invasive protein delivery systems using liposomal carriers. Liposomes have been widely used for many years not only in drug delivery systems but also in various cosmetic applications including delivering vitamins, ceramides, antioxidants, or growth factors. Not only they help deliver the encapsulated substance into the deeper layers of the skin, they also provide an additional protection to the substance. The substance is stabilized by the liposome and is thus less prone to oxidation and its shelf life can be prolonged [3].

The aim of this diploma thesis is to describe the process of encapsulation of fibroblast growth factor-2 into liposomes to enhance its transdermal penetration efficiency and extend its lifetime. Characterization of the prepared encapsulated growth factors and their physical and chemical properties will be measured and discussed.

2 THEORETICAL PART

2.1 Skin structure

To fully understand the drug delivery methods, skin structure and its properties need to be discussed first. Skin is the biggest organ in the human body and plays an important role in protecting the internal environment and enhancing a person's health. It protects the body by blocking harmful elements, i.e., bacteria, viruses, ultraviolet (UV) irradiation, and toxic chemicals from the environment from entering the body. Therefore, the skin barrier is essential to protect our health. On the other hand, it is possible to use our skin to deliver therapeutic substances into our body by overcoming the excellent barrier properties of the outermost layer of the skin in some cases, where invasive or peroral methods of drug delivery are not possible [3, 4]. The skin is composed of the outermost layer, epidermis, dermis, and the hypodermis. The outermost layer of the epidermis consists of 10–15 layers of corneocytes (dead skin cells).

The epidermis is an avascular layer of the skin but is penetrated by sensory nerve endings and is firmly locked to the underlying dermis by *epidermal pegs*. In the deeper layers, cells are living and actively proliferating and throughout their lifetime are gradually passing to the skin surface during which they are getting *keratinized* and then shed from the skin surface. The epidermis is composed of many layers of cells as displayed in Figure 1, being from outwards inside the *stratum corneum* (SC), *stratum lucidum, stratum granulosum, stratum spinosum* and *stratum basale* [5].

The bottom layers *stratum basale* and *spinosum* are referred as the germinal zone, where new cells are produced continuously to replace the shed cells. As the cells approach the *stratum granulosum* through the *stratum spinosum* and *basale*, they become flattened. Once they reach the *stratum granulosum*, the process of keratinization starts and as the cells approach the upper layers, they are in a process of dying. Thus, the upper layers (*corneum, lucidum, granulosum)* are referred together as the horny layer of the skin [5].

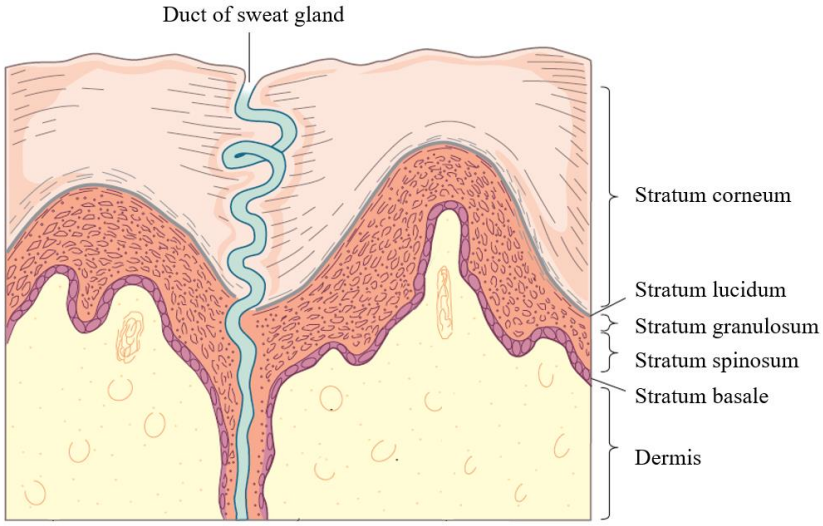

Figure 1 Structure of the upper skin layers of the epidermis and dermis [5]

The dermis is a deeper layer of the skin, it represents a greater part of the total thickness of the skin. As well as the epidermis, the dermis can be divided into two finely textured layers – *papillary* and a *reticular* layer. The papillary layer is closely packed with the

epidermis and the reticular layer gradually blends into the hypodermis and the connective tissue. The reticular layer gives the skin its strength, elasticity, and toughness. Major part of the dermis is formed by an interweaved extracellular matrix (ECM) of collagen and elastin fibres and the extrafibrillar matrix composed of proteoglycans with glycosaminoglycan chains (i.e., hyaluronic acid), fibronectins binding the numerous components of the ECM and laminins which influence a cell's adhesion, proliferation, differentiation, migration, and growth (Figure 2) [6].

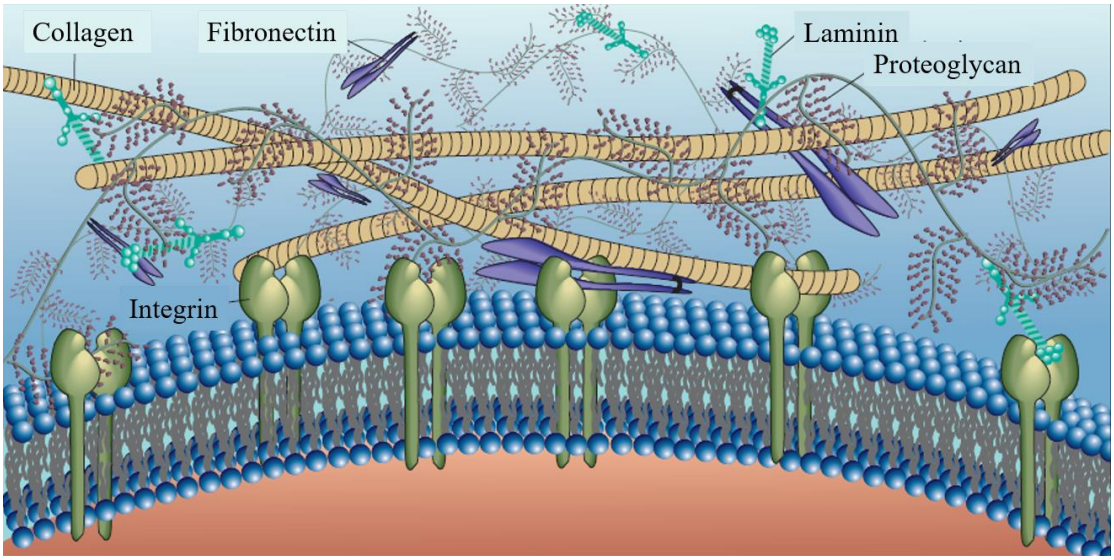

Figure 2 Macromolecular organisation of the extracellular matrix and connection with the phospholipid bilayer of the cell membrane [6]

Three major cell types are found in the dermis – fibroblasts, macrophages, and mast cells. Fibroblasts represent the connective tissue cells in the skin that inhabit and produce the extracellular matrix within the dermis. They manufacture collagen as well as other macromolecules of its matrix intracellularly and then secrete them by exocytosis. After being secreted, these macromolecules assemble into bigger aggregates. In the case of collagen, the cell secretes only a precursor of collagen, procollagen, which is a polypeptide chain with additional peptide extensions at the terminal positions of the chain to prevent premature assembly into collagen fibrils inside of the fibroblast. These end peptides are cut off after secretion by the extracellular enzymes to allow the assembling of the polypeptide chains into the collagen molecules into tripple helix and then into collagen fibrils in the outer space of the fibroblast. Macrophages on the other hand are phagocytic cells, they secure protection against infection by ingesting damaged or dead cells as well as helping combat infection. They are also vital for tissue growth, repair, and renewal – where fibroblasts are crucial for extracellular matrix production, macrophages secure extracellular cell degradation [7].

The fibrous part of the dermis imparts elasticity to the skin and makes it fairly hydrophobic unlike SC. Thanks to the hydrophobic nature of the dermis, polar molecules, such as peptides and proteins can easily penetrate through it. Dermis is interlaced with blood and lymphatic vessels and nerves [8].

The deepest layer of the skin – hypodermis – is formed by loosely arranged connective tissue containing elastic fibres and fat. Hypodermis is richly supplied with nerves and contains lymphatic and blood vessels, sensory endings, and roots of hair follicles [5].

2.2 Transdermal delivery of peptides and proteins

In dermatological diseases and serious wound case treatment, topical delivery of the therapeutic agent or drug is the most common approach. These therapeutic agents widely contain various proteins and peptides since they are able of curing a variety of indications. A large number of peptides and proteins undergo degradation by proteolytic enzymes in the gastrointestinal tract and thus oral delivery is not possible. Enzymatic degradation also occurs when peptides and proteins are administered via a nasal or ocular route [8].

Thus, the parenteral route is always favourable in regard to proteins and peptides. Nevertheless, many proteins and peptides have a very short half-life, repeated administration to the patient is necessary. In these cases, transdermal delivery offers a noninvasive, painless, and easily repeated and accessible administration of the therapeutic agent. However, as mentioned earlier, the penetration depth of the therapeutics is hampered by the SC properties and hence the maximal daily dose delivered through this route is 5–10 mg [8, 9]. However, not every therapeutic agent is suitable for transdermal delivery, there are several factors the agent needs to meet: daily dose at a maximum of 20 mg, the molecular weight under 500 Daltons, lipophilicity (logP) in the range 1–3, melting point below 200 °C and maximum of 2 hydrogen bonding groups. Of course, the agent should not be irritative for the skin and should not stimulate an immune reaction directly [10].

It was reported that noninvasive lipid-based nanoparticle delivery systems can penetrate through the SC into the epidermal and dermal layers of the skin. The cell membrane and liposomes share a similar structure. The building block of the cell membrane is a lipid bilayer of phospholipids, sphingolipids, and cholesterol with phospholipids being the most abundant type of lipids in the lipid film. Beside lipids, another component of the membrane are large globular proteins which can either be integral (penetrate all way through the lipid bilayer) or peripheral (protrude from the bilayer surface and do not penetrate through) as displayed in Figure 3.

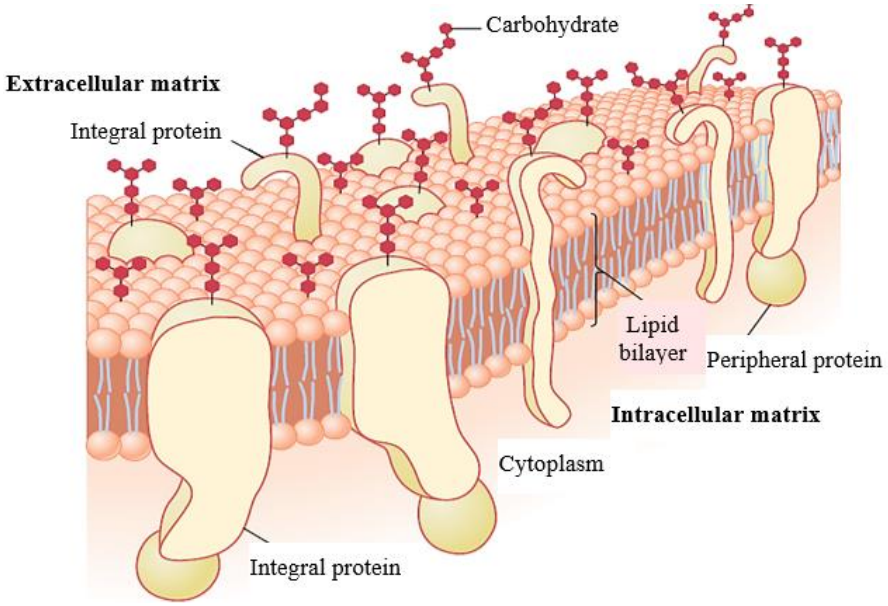

Figure 3 Structure of the cell membrane, showing the main components being the phospholipid bilayer, proteins, and carbohydrates [11]

The outside surface of the cell is covered in a loose carbohydrate coated *glycocalyx* formed by *proteoglycans* (carbohydrate chains bound to a small protein core), *glycoproteins* (carbohydrate chains attached to an integral or peripheral protein) and *glycolipids* [11].

Liposomes are as well formed by a lipid bilayer and their detailed structure will be further discussed in chapter 2.3. Lipid-based nanoparticles, due to their lipid nature similar to the cell membrane, their biodegradability, small size, and deformability, represent a promising skin drug delivery system [12].

Lipid-based nanoparticles can also hydrate the skin and allow rearrangement of the skin cells themselves, even when the therapeutic agent is not present. This can either lead to penetration enhancement of the nanoparticles or to increased interaction rate between the nanoparticles and the SC [13]. Regarding the first case scenario, topically applied nanoparticles can penetrate the skin by three potential pathways as displayed in Figure 4 – the appendageal route, the intracellular route, and the intercellular route [14].

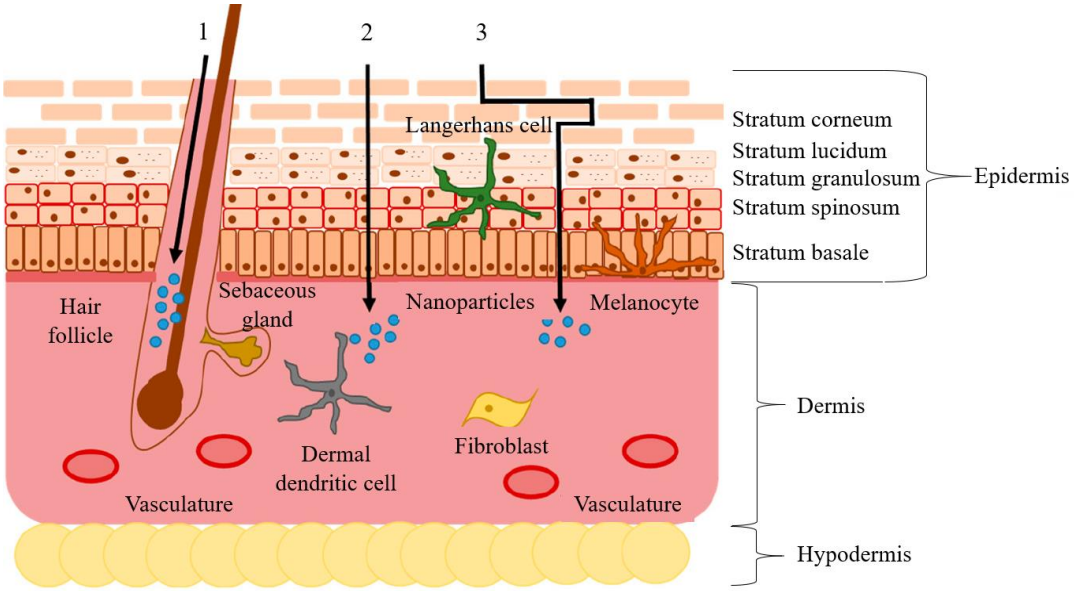

Figure 4 Penetration pathways of nanoparticles: the appendageal route (1), intracellular route (2) and intercellular route (3) [14]

The appendageal route involves penetration via sebaceous glands or hair follicles [14]. The intracellular or transcellular route leads straight through the corneocytes in SC. Even though corneocytes are of polar nature due to the presence of hydrated keratin matrix, the intercellular route includes penetration via the lipophilic domains surrounding the corneocytes as well meaning the permeation is done by repeated portioning between the polar corneocyte and lipophilic environment.

The intercellular route, on the other hand, leads through the intercellular lipid domains around the corneocytes, where transport can take place either by diffusion via the lipid tails or by diffusion via their polar head groups. Therefore, polar permeants would most likely diffuse through the polar heads while less polar permeants would diffuse via the lipid pathway, but the main penetration route highly depends on the physicochemical properties of the permeant [15, 16]. However, it is accepted that the appendageal route contributes to only 0.1 % of the permeation area and therefore their contribution to drug

delivery is minor. Therefore, most of the transdermal delivery strategies are focused on the enhancement of inter and intracellular delivery routes [9].

Therefore, encapsulation of therapeutic proteins or peptides into lipid-based particles such as liposomes, ethosomes, niosomes, and transferosomes offers an attractive solution for protein and peptide delivery to and across the skin [8]. A number of physicochemical properties such as particle size and size distribution of the particles, solubility, release mechanisms, lipid composition, lamellarity, and the charge of the liposomal surface influence the drug release in different skin layers [17]. Therefore, it is essential to consider selection of the right encapsulation technique based on the required vesicle size and nature of the core.

2.3 Liposomes

Liposomes are the most reported lipid-based nanoparticle delivery systems. The name liposome comes from Greek words *lipos* (fat) and *soma* (body) and were studied as the first possible drug delivery carrier for the purposes of delivering drugs into the skin because of the similarities with human skin structure as discussed earlier in chapter 2.2. These microscopic spherical lipid vesicles occur naturally in human milk and are usually 0.05–5.0 μm in diameter, but the size depends on the preparation method [17, 20].

Conventional liposomes are formed by natural phospholipids and cholesterol. Molecules of phospholipids are amphiphilic – they consist of a hydrophilic polar head and two hydrophobic nonpolar hydrocarbon tails usually formed by fatty acids with one tail being unsaturated. Since the tails are of hydrophobic character, they are easily repelled by water to form a layer where the polar heads face water and the tails face away from the water [17]. The hydrophobic tails of one layer interacts with Van der Waals interactions with tails from another layer forming a bilayer sheet spontaneously (Figure 5). Formation of closed bilayers follows.

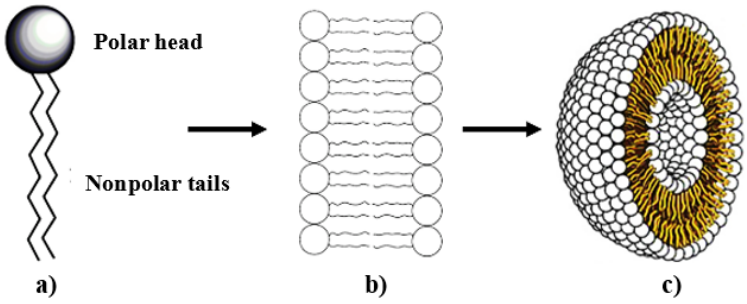

Figure 5 Formation of liposomes (c) from phospholipid molecule (a) and phospholipid bilayer sheet (b) in aqueous solution [17]

The aqueous core is trapped inside the lipid bilayer vesicle and due to the presence of water, various hydrophilic therapeutic proteins, diagnostic agents, or cosmetic actives can be trapped into the core of the liposome [17, 20]. If the drug is of lipophilic character, it is entrapped into the lipid bilayer [2]. When amphiphilic and lipophilic drugs are being encapsulated, liposomes play a role of an organic solvent and therefore, a larger concentration of the drug can be applied [21].

Phosphatidylcholine (PC) extracted either from egg yolks or soybeans is used frequently in drug delivery applications, but other types of natural phospholipids are also used quite

often, such as phosphatidylethanolamine, phosphatidylserine, phosphatidylglycerol or phosphatidylinositol. Depending on the structure of the phospholipid, various liposome characteristics can be obtained resulting in different interactions with the skin [17]. Moreover, each phospholipid type has a different phase transition temperature (T_M), which is a parameter affecting the liposome stability, encapsulation efficiency, and storage stability. When the ambient temperature is higher than the T_M of a certain phospholipid, it occurs in a fluid state which is convenient during drug entrapment into the liposome. Phospholipids with T_M higher than body temperature are often used in drug delivery carriers for *in vivo* applications, liposomes are more rigid and remain in a gel state. Using a phospholipid with T_M lower than the body temperature may lead to instability of the system and premature liposome disintegration [18].

Another structural component of liposomes is cholesterol. Even though it cannot form a bilayer on its own, it is incorporated into liposomes to reduce the permeability of the membrane to molecules soluble in water, to stabilize the membrane and to decrease the fluidity of the biomembrane of phospholipids with low T_M. Cholesterol can increase the drug entrapment percentage and liposome rigidity, but it can also result in a rise in diameter of the liposomes, which might not be beneficial in certain applications [17, 19].

Except the phospholipids and cholesterol mentioned above, other substances can be incorporated into the liposome structure. It is possible to use modified lipids, where the first acyl hydrocarbon chain is grafted with a polyethylene glycol (PEG) chain to obtain PEGylated lipids. These lipids are commonly used in applications, where the half-life of the encapsulated drug needs to be prolonged, i.e., in cancer therapy. Due to the PEG coating on the liposome surface, the retention time is increased [17, 20]. Liposomes are generally more tolerated than synthetic polymers, however, they often undergo degradation due to enzymatic activity. Polymer/liposome composite systems or even liposomes based on synthetic polymers exhibit controlled release of the encapsulated drug and enhanced stability of the whole system [20].

2.3.1 Types of liposomes

Liposomes can be categorised by different criteria such as diameter of the vesicles, number of lipid bilayers, or charge.

2.3.1.1 Types of liposomes based on size

Liposomes are always formed by at least one closed lipid bilayer – unilamellar vesicles (ULV). Depending on the size, these can be divided into small unilamellar vesicles (SUV), large unilamellar vesicles (LUV), or giant unilamellar vesicles (GUV) but these are used for the most part only in research work to model biological membrane. If more than one lipid bilayer is present, these are then referred as multilamellar vesicles (MLV) with an onion structure.

MLV are formed from ULV when another smaller unilamellar layer is formed inside of the first ULV, forming concentric lipid spheres with time. Each layer is separated from the other by a layer of water. MLVs can also occur without the concentric onion structure, but these are not used as often because they are rather large (in the range of 1,000 nm), represented in Figure 6 [21, 22].

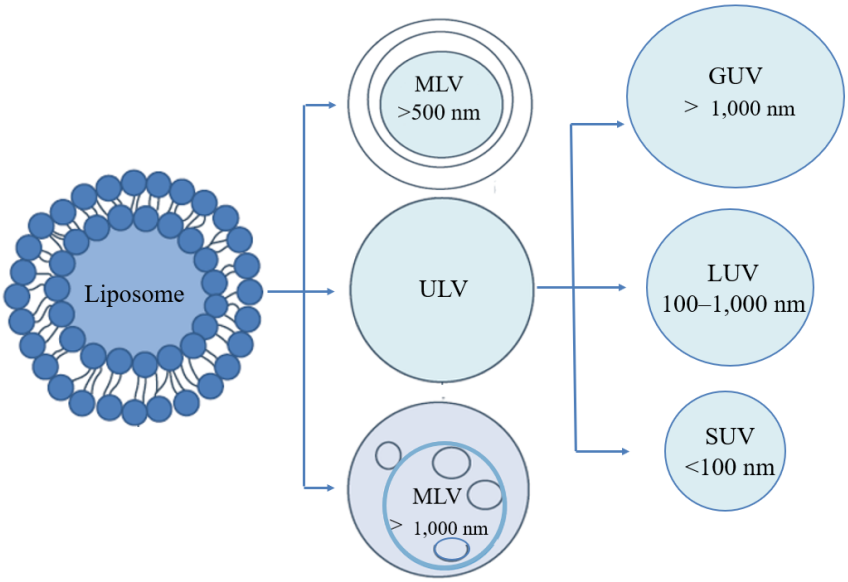

Figure 6 Types of liposomes based on structural parameters [17]

2.3.1.2 Types of liposomes based on charge

Liposomes can be neutral or charged. Mammalian cell membranes are negatively charged, therefore the interaction with neutrally charged liposomes is negligible. In such cases, the drug can enter the cell only after extracellular release from the liposome [18, 23].

Cationic liposomes are composed of cationic lipids and are suitable for the delivery of negatively charged nucleic acids such as deoxyribonucleic acid (DNA) or ribonucleic acid (RNA) due to the electrostatic interaction between the vesicle and the cell. Electrostatic interactions also support the encapsulated substance through the negatively charged cell membrane [18, 24]. A large amount of anionic lipids is found in the lipid lamellae of the SC that can interact with cationic liposomes effectively. However, it was indicated that cationic vesicles are rather cytotoxic and tend to damage the skin compared to negatively charged liposomes [25]. Therefore, they are restricted only to local administrations [17].

Anionic liposomes, depending on the encapsulated drug, are reported to be more stable which results in increased intracellular uptake and penetration enhancement. They also do not irritate the skin as cationic liposomes and thus give safety and efficiency [25]. In any case, charged liposomes tend to be more stable than neutral liposomes due to the electron repulsion between the liposome particles when stored in the dispersion medium for longer periods [17].

2.3.1.3 Types of liposomes based on structure of the system

Depending on the structure and composition of the vesicular system and its application, different liposome types are applicable: from conventional liposomes to ethosomes, niosomes, transferosomes, proniossomes, all mentioned above will be discussed further. When these types of liposomes are used, the system is intended for a specified application [2, 3].

Liposomes composed only of phospholipids and cholesterol are referred as c*onventional liposomes*. These are the simplest liposomes with negatively charged or neutral

phospholipids. They can vary in size, surface charge, or in fluidity of the bilayers [17]. Unfortunately, conventional liposomes are not able to penetrate the skin enough to reach the epidermis and dermis regions to deliver the drug. They usually accumulate in the outermost layer of the skin in SC, but only a small number of conventional liposomes can penetrate the SC via hair follicles. Therefore, they do not penetrate the skin or enhance its permeability [3]. The reason why conventional liposomes are not able to penetrate deeper layers of the skin sufficiently is that they tend to adhere to the cell walls in the SC. The phospholipid-associated bonds collapse which leads to leaking of the encapsulated drug before reaching deeper layers of the skin [3, 26].

Just like conventional liposomes, *ethosomes* are noninvasive drug delivery systems based on phospholipids, cholesterol, water, and alcohol such as displayed in Figure 7. In contrast to conventional liposomes, ethosomes can penetrate into deeper layers of the skin even into the basal skin layer and blood circulation [27, 28] due to relatively high (20–50 %) ethanol or isopropyl alcohol content which makes them rather soft and easily deformable [29, 30]. This level of elasticity and flexibility is not commonly found in conventional liposomes and ensures facile intracellular penetration through the SC due to the osmotic gradient between the outer and inner layers of the SC [32].

Ethosome vesicles usually show smaller diameters than conventional liposomes, depending on the method of preparation, in the range of tens of nanometres to a few microns [32]. This reduction in size comes from the conferment of a net negative charge by ethanol onto the vesicle surface and therefore, the vesicle size decreases with increased ethanol content [33]. They also offer higher entrapment efficiency of the therapeutic agents and improved stability of the whole system [34]. The penetration enhancement of ethosomes is not based only on their small size and flexibility, ethanol can also affect as a penetration enhancer. Ethanol enters the intracellular space between the corneocytes in the SC, where it reduces the T_m of the cell membrane lipids in the SC leading their fluidization [35]. This results in disturbance of the lipid bilayer arrangement and thus the density of the intracellular space is reduced. The ethosomal vesicles can then undergo the intracellular permeation route into deeper layers of the skin effortlessly where they fuse with the skin lipids and release the encapsulated substance [33]. One major advantage of ethosomal carriers is the possibility to entrap and deliver large bioactive molecules such as proteins and peptides [36]. The entrapped molecule should always be of high effectiveness at low doses (10 mg/day) and highly lipophilic to achieve satisfactory results in topical administration [28, 31].

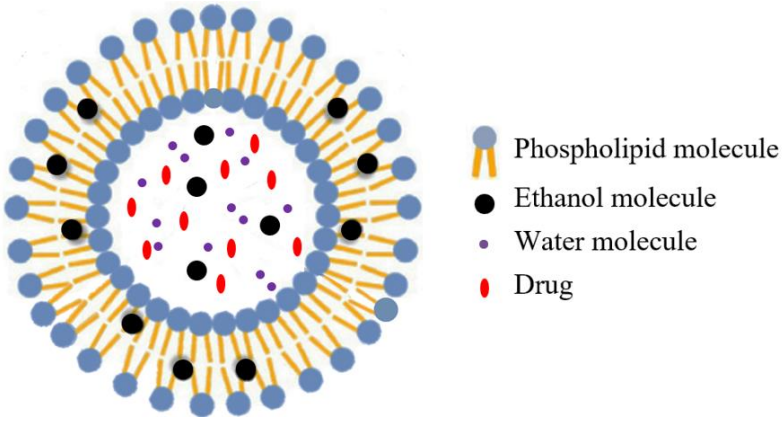

Figure 7. Schematic structure of the ethosome carrier system [29]

Another kind of deformable vesicles represent *transferosomes* which are always composed of four key elements – phospholipids, ethanol (in concentrations usually below 10 %), water, and a destabilizing agent i.e., edge active surfactant. The edge activators are incorporated into the membrane of the vesicle, commonly used are single chain surfactants such as sodium cholate, sodium oleate, sodium deoxycholate, and various nonionic surfactants (Span® 80 or Tween®80) [37]. Since transferosomes are ultra-deformable, an elastic intracellular route is possible through the channels in SC without disruption of the vesicle if the vesicle diameter is below 300 nm and the trans-epidermal osmotic gradient is maintained [38, 39]. Phospholipids contained in transferosomes give the vesicle a hydrophilic surface and hence, transferosomes tend to migrate into deeper and better hydrated skin layers from the skin surface through the SC into deeper epidermal and dermal layers intact. The elasticity and high deformability of the vesicles result from the high radius of curvature of the system provided by the edge activator. These are usually present in the concentration between 10–20 %, but there is always a risk of micelle formation with the edge activator concentration greater than 15 % [40]. Since transferosomes are made of natural phospholipids, they are biocompatible vesicles with high entrapment efficiencies up to 90 % when a lipophilic drug is encapsulated. They can hold low as well as high molecular weight active substances, protect them from metabolic degradation, and secure their slow and gradual release. Therefore, transferosomes are also quite suitable for protein and peptide transdermal delivery [41].

Niosomes and conventional liposomes are both amphiphilic vesicles with similar structure, properties, and pharmaceutical applications. However, the main ingredients of niosomes are nonionic surfactants, rather than phospholipids, which are the main component of conventional liposomes. The nonionic surfactants give niosomes higher stability and entrapment efficiency but can also affect size, rigidity, pharmacokinetics, and pharmacodynamics. Depending on the application area, we can prepare niosomes with tailor-made properties just by selecting the most suitable surfactant and preparation method. Commonly used surfactants include terpenoids (i.e., squalene), polysorbates, or alkyl ethers [8, 42]. In the case of niosomes, the fluid membrane of the vesicle with high elasticity is not obtained as there is in transferosomes [43]. To enhance the niosome stability, efficacy, and drug load, charged molecules or ionic amphiphiles are also generally added. Niosomes can be prepared as unilamellar as well as multilamellar vesicles in the sub-micron size range, depending on the lamellarity level [21, 44]. The main advantages of using niosomes over liposomes are lower costs for preparation but at the same time, obtaining a material with similar stability and biocompatibility, penetration properties, and encapsulation efficiency [45, 46]. A type of niosomes are *proniosomes*, which contain the carrier and a surfactant deprived of water. Hydration of proniosomes results in the formation of niosome dispersion. This approach solves the problem of aggregation, fusion, and leaking associated with the formation of niosomes [47].

2.3.2 Drug release from liposomes

Liposomes in general can be used to deliver hydrophilic (water soluble) as well as lipophilic (lipid soluble) drugs. The hydrophilic drugs are encapsulated inside the aqueous core of the liposome, whereas the lipophilic drugs are carried in the liposome membrane formed by phospholipid bilayers. [48]. After the application of liposomes in dosage form onto the skin surface, liposomes are released and diffuse through the SC into deeper skin layers and tissues depending on their relative solubility in each environment.

The penetration speed is given by the liposome properties including their molecular size, melting point and solubility, viscosity, and potential binding with the environment and the encapsulated drug [16].

Liposomes can interact with skin cells in various manners. Liposomes can adsorb to the cell surface by weak hydrophobic or electrostatic forces resulting in drug release from the cell. Since their structure is similar to the wall and cell membranes, the fusion with them by insertion of the liposome bilayer into the membrane cell and simultaneous drug release into the cytoplasm is possible as well (Figure 8). Drugs can be released from the liposome also through endocytosis by mononuclear phagocyte system cells such as macrophages or neutrophils [17, 49, 50].

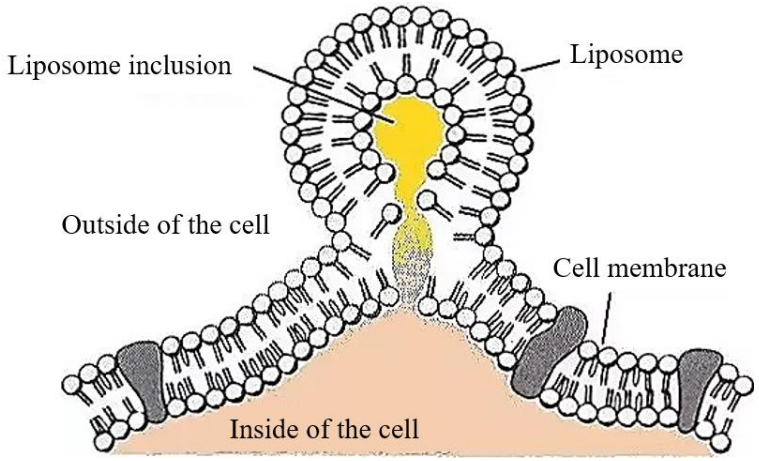

Figure 8 Fusion of phospholipids in the liposome membrane with a membrane of the cell facilitates the entrapped drug entry into the cell interior [48]

2.3.3 Liposome stability

Liposomes help stabilize and prolong the shelf life of encapsulated substances, but in fact, liposomes themselves tend to have limited shelf life resulting from their physical, chemical, and biological stability.

Physical stability of the liposomal system includes the appearance of liposomes, their average size, and size distribution. These properties can be determined using transmission electron microscopy (TEM), dynamic light scattering (DLS), and the physical stability of the liposomal colloidal suspension can be determined by measuring the change in *zeta potential* [51]. When a physically stable liposome is formed, both the size distribution and the amount of encapsulated substance are preserved. Physical stability of the system can be improved by using fresh materials and solvents, avoiding high temperatures, and working under an inert atmosphere [52]. Chemical stability of liposomes changes with time rapidly due to the presence of phospholipids in their structure containing unsaturated fatty acids. Liposomes can undergo chemical degradation through oxidation of the unsaturated hydrocarbon tails or through hydrolysis of the ester bonds [51].

Even though the liposomal structure resembles a biomembrane structure, liposomes are still recognized by the phagocytic system in the blood stream. Therefore, the *in vivo* plasma half-life stability of the liposome drug system needs to be improved. This biological stability issue can be solved by using microencapsulation techniques or coating the liposome particles with polyethylene glycol or chitin derivatives [52, 53].

The stability of the liposome protein or liposome-peptide system varies depending on the encapsulation technique, selected phospholipid type, and properties of the protein or peptide. The encapsulation of such substances can lead to their deactivation via a change in structural conformations and thus minimizing their therapeutic function. This disruption occurs during encapsulation of proteins in the primary through quaternary structure due to oxidation, denaturation, aggregation, or precipitation of the protein or due to pH alternation. The pH alternation during the encapsulation process can affect groups on the protein chain with pK_a similar to the initial pH. The hydrophobicity or the hydrophilicity of the protein relates to its ability to nest inside the aqueous liposome core. This thesis focuses on the encapsulation of the fibroblast growth factor-2 which is a hydrophilic protein and thus liposome preparation and stability evaluation methods will be performed accordingly [54, 55].

2.4 Fibroblast growth factor-2

The fibroblast growth factor-2 (FGF2), also known as basic fibroblast growth factor (bFGF), was first isolated from the pituitary. It belongs to a large FGF family of at least 21 structurally related proteins that regulate a number of crucial biological processes [56]. Even though these FGFs are structurally similar, the FGF2 subfamily differs in many ways, i.e., most of the FGFs are secreted through the Golgi secretory pathway (through the endoplasmic reticulum), FGF-2 is secreted separately.

2.4.1 Structure

Crystalline FGF-2 has a homologous core region that consists of 146 amino acids. These are ordered into 12 antiparallel β-sheets (β_1–β_{12}) flanked by different carboxyl and amino ends (Figure 9) arranged in a trigonal pyramidal manner [57, 58]. The surroundings of the β_1– β_2, β_{10} and β_{12} are involved in the binding of heparin and heparan sulfate [57]. These specific areas of FGF2 were found by analysing the crystal structure of FGF-2 complexed with hexasaccharide fragments of heparin (because heparin itself is too heterogenous and not compatible with crystallization) [59, 60].

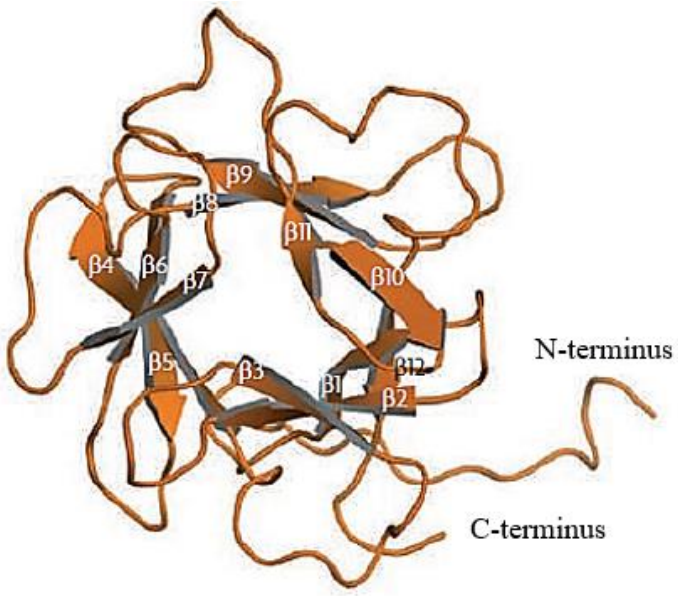

Figure 9 Structure of fibroblast growth factor, showing its 12 antiparallel β-sheets with amino and carboxyl ends [57]

The FGF2 contains four cysteine residues, however, there are no intramolecular disulfide bonds. It also contains a large number of basic residues giving the isoelectric point of 9.6 [61]. FGF2 exists in multiple isoforms in humans and mice, these are generated from a single messenger RNA (mRNA) by alternative translation. Until now, one low molecular weight (18 kDa) and three high molecular weight (22, 22.5, and 24 kDa) forms have been identified. The low molecular weight form is found in the cytosol, that is able to activate FGF receptors (FGFRs) on the cell surface. On the other hand, high molecular weight forms are mostly localized in the nucleus and regulate gene transcription and initiate proliferation. Therefore, depending on the localization in the cell, different molecular weight proteins with different biological functions occur [59, 62].

2.4.2 Receptors

Every FGF-stimulated process is mediated by FGFRs and is tightly regulated. One low-affinity and four high-affinity receptors are distinguished. The representative of the low-affinity receptor is a heparan sulfate (HS) proteoglycan. The HS is a linear sulphated polysaccharide belonging to the group of glycosaminoglycans. It is critical for FGF signalling. When removed enzymatically from the cell surface, the biological activity of FGF abolishes. Not only it ensures the activity of FGFs, the HS-FGF interaction also results in the protection of the FGF against acid and heat denaturation and protease cleavage [59, 62].

The four high-affinity FGFRs 1–4 are similar in their structure and work as tyrosine kinase receptors. The interaction of these FGFRs leads to dimerization of receptor monomers and activation of intracellular kinase domains. Of all of these four FGFRs, FGFR-1 has the highest affinity when bound to FGF2 [62, 63, 64].

2.4.3 Biological function

Fibroblast growth factor-2 is a mitogenic cytokine protein affecting their specific target cells to grow and/or differentiate. Human FGF2 serves as a pleiotropic regulator of differentiation, migration, and maintenance of stem cells, including human pluripotent cells, where it helps them to maintain the pluripotent state [65, 66].

FGF2 is a multifunctional growth factor with various effects in different cells and tissues. It plays significant roles in remodelling, diabetic ulcer healing processes [67], bone regrowth [68] and cartilage repair [69], periodontal tissue regeneration [70] and even treating major depressive and mood disorders [57].

Since FGF2 plays a key role in various cellular activities, stimulates growth and proliferation, and thus enhances tissue regeneration, it has been shown to decrease the appearance and depth of wrinkles [71] and scars [72] by increasing the elasticity and hydration of the skin, it also promotes hair growth by promoting papilla cell proliferation and thus increasing the size of hair follicle [73].

For the applications mentioned above, stem cell culturing and protein therapy, long-term maintenance of the FGFs is required. Naturally occurring (wild type) FGFs have usually low thermal stability and limited half-life. Stability of FGF2 highly depends on its environmental factors, it degrades rapidly with surrounding temperature above 40 °C and pH lower than 5 [74]. It was also discovered that the amount of wild type FGF2

decreased by more than 50 % in around 4 hours after initial feeding and after 24 hours there was almost none FGF2 present [66].

Nowadays, stabilized growth factors-2 (FGF2-STAB®) are manufactured. Due to the stabilization of FGF2 by computationally searching for mutations with minimized Gibbs free energy of the native state, FGF2-STAB® retains its full biological activity even after 20 days at 37 °C [65]. The FGF2-STAB® is therefore much more suitable for the FGF2 application field.

2.4.4 Wound treatment using FGFs

FGF2 is quite unique, unlike other FGF types, FGF2 is expressed in a variety of tissues. It was shown to induce dermal and epidermal repair process as well as having a wound healing effect unlike any of the 20 other FGFs from the family. It was suggested [75] that FGF2 has an anti-scarring effect via fibroblast apoptosis induction in the granulation tissue and thereby is beneficial in wounds that are difficult to cure, such as diabetic ulcers or wounds after tumour resection surgery [76]. Even though the therapeutic effect of FGF2 is mesmerizing, its stability, on the other hand, is an obstacle affecting its application area. The *in vivo* half-life is about 1.5 min and its activity decreases rapidly due to diffusion and enzymatic degradation. To prolong its half-life and decrease the risk of degradation in *in vivo* applications, FGF2 can be stabilized when encapsulated into liposomes. Furthermore, liposomes provide a moist environment on the wound surface, which is vital for scar-free tissue regeneration [77, 78].

3 AIM OF THE THESIS

The aim of this diploma thesis is to prepare FGF2-STAB® loaded liposomes that are suitable for transdermal drug delivery. The aim of the thesis includes theoretical research on transdermal delivery of lipid-based particles and liposomes, specifically, their type, release mechanisms, and stability as well as research on FGF2-STAB®.

Prepared FGF2-STAB® loaded liposomes would be tested on:

1) Stability and charge via zeta potential measurements
2) Liposome diameter and particle size distribution via DLS
3) Encapsulation efficiency

Liposomes intended for transdermal delivery of FGF2-STAB® ought to be stable (zeta potential out of the ±30 mV range, preferably with negative charge), relatively small with diameters around 100 nm and with encapsulation efficiency at least 60 %.

Measured data would be further evaluated and discussed and conclusions would be made.

4 EXPERIMENTAL PART

4.1 Chemicals

All chemicals were used without further modification or purification.

Chemicals for liposome preparation:

- L-α-Phosphatidylcholine (PC) from egg yolk, ~60 % (TLC), CAS: 8002-43-5, Sigma-Aldrich (Prague, Czech Republic),
- Cholesterol, sigma grade ≥ 99 % Sigma-Aldrich (Prague, Czech Republic),
- Dichloromethane G.R. stabilized Lach-Ner L.t.d. (Neratovice, Czech Republic),
- Stable fibroblast growth factor (FGF2-STAB®) was provided by Enantis L.t.d. (Brno, Czech Republic),
- Liquid nitrogen (99.999 %) was purchased from Linde Gas, a.s. (Brno, Czech Republic).

Chemicals for phosphate saline buffer (PBS) preparation:

- Potassium phosphate monobasic (KH_2PO4), for molecular biology ≥ 98.0 % Sigma-Aldrich (Prague, Czech Republic),
- Potassium phosphate dibasic (K_2HPO_4), reagent grade biology ≥ 98.0 % Sigma-Aldrich (Prague, Czech Republic),
- Sodium chloride (NaCl) G.R. Lach-Ner L.t.d. (Neratovice, Czech Republic),
- Phosphoric acid (H_3PO_4), 85 % p. a. PENTA s.r.o. (Chrudim, Czech Republic),
- Potassium hydroxide (KOH) pellets A.G., CAS 1310-58-3 Penta s.r.o. (Praha 10, Czech Republic,
- Ultrapure water type II according to ISO 3696.

Chemicals used for liposome characterization:

- Bradford Reagent for 0.1–1.4 mg · ml^{-1} protein for UV-VIS measurements Sigma-Aldrich (St. Louis, Missouri United States of America).

4.2 Equipment

- Analytical balance SI-234A, DENVER INSTRUMENT (Denver, Colorado United States of America).
- Water purification system Direct-Q ®, Merck (Kenilworth, New Jersey United States of America).
- IKA® RET control-visc magnetic stirrer, IKA®-Werke GmbH & Co. KG (Staufen, Germany),
- Centrifuge 5804 R, Eppendorf (Říčany u Prahy, Czech Republic).
- UV-VIS spectrophotometer V-730, Jasco (Tokyo, Japan).
- Zetasizer Nano ZS, Malvern (Grovewood Road, United Kingdom).

- Single use cuvettes for UV-VIS, product code 1938
  Kartell S.p.A. – LABWARE Division (Noviglio, Milano, Italy).
- DynaPro® NanoStar® dynamic light scattering instrument
  Wyatt Technology Corporation (Santa Barbara, California United States of America).
- Scanning Electron Microscope with E-beam writer TESCAN MIRA3Raith LIS (MIRA),
  TESCAN (Brno, Czech Republic).
- Carbon films on 200 Mesh copper grids, Pack of 25, product code AGS160H, Agar Scientific L.t.d. (Standsted, Essex, United Kingdom).
- Laboratory ultrasonic cleaner, Ultrazvuk, S.r.o. (Hradec Králové, Czech Republic).
- Avanti® Polar Lipids, Inc (Alabaster, Alabama United States of America), Mini-Extruder set, set includes:
  - Mini-extruder holder,
  - Mini-extruder,
  - 2 × Hammilton 1 ml syringes,
  - Filter supports,
  - Polycarbonate membranes with pore size:
    - 200 nm,
    - 100 nm.

4.3 Encapsulation of FGF2-STAB® into liposomes

4.3.1 Phosphate buffer saline recipe

For the preparation of empty liposomes and liposome hydration, a solution of 20 mM potassium phosphate buffer and 750 mM sodium chloride buffer with pH 7.5 was used. Components for PBS preparation were added to a 500 ml borosilicate glass bottle according to Table 1, dissolved in 200 ml of ultrapure water and then the ultrapure water was added to the total volume of 500 ml at room temperature. The pH was adjusted to 7.5 using 1 M KOH solution and 1 M H_3PO_4 solution.

Table 1 Mass and concentration of components for PBS preparation

PBS component	Mass [g]	Concentration [mM]
K_2HPO_4	1.43	16.4
KH_2PO_4	0.25	3.6
NaCl	4.38	750.0

4.3.2 Liposome preparation

Empty (LIP) and FGF2-STAB® loaded liposomes (FGF2-LIP) were prepared using the reverse phase evaporation method. Phosphatidylcholine and cholesterol were used in the molar ratio (4:1). Briefly, an amount of 163 mg of phosphatidylcholine and 40.8 mg of cholesterol was dissolved in 5 ml of dichloromethane in a round bottom flask. In the case of the FGF2-STAB® loaded liposomes, the amount (according to Table 2) of FGF2-STAB® solution in PBS pH 7.5 with concentration 1 mg/ml was added to the dissolved lipid solution. In the case of LIP, the FGF2-STAB® solution was substituted with the same amount of PBS pH 7.5. This solution was further homogenized using

a laboratory ultrasonic bath (cycle with 10 s on and 10 s off) in ice water (3 °C) until a water in oil (w/o) emulsion is formed.

Table 2: Preparation of FGF2-LIP with different FGF2-STAB® quantity

Formula	Phosphatidylcholine to FGF2-STAB® ratio	FGF2 loading [mg]	FGF2-STAB® concentration in formula [µg/ml]
1	2,000:1	82	40.8
2	1,500:1	109	54.3
3	1,000:1	163	81.5
4	500:1	326	163.0
5	300:1	543	271.7

In the next step, the dichloromethane was evaporated from the emulsion using the high vacuum line (Figure 10), until a viscous lipid hydrogel was formed. This lipid hydrogel was hydrated using 2 ml of PBS pH 7.5 at laboratory temperature for 18 hours and sonicated using the same procedure as described beforehand for a total of 5 minutes.

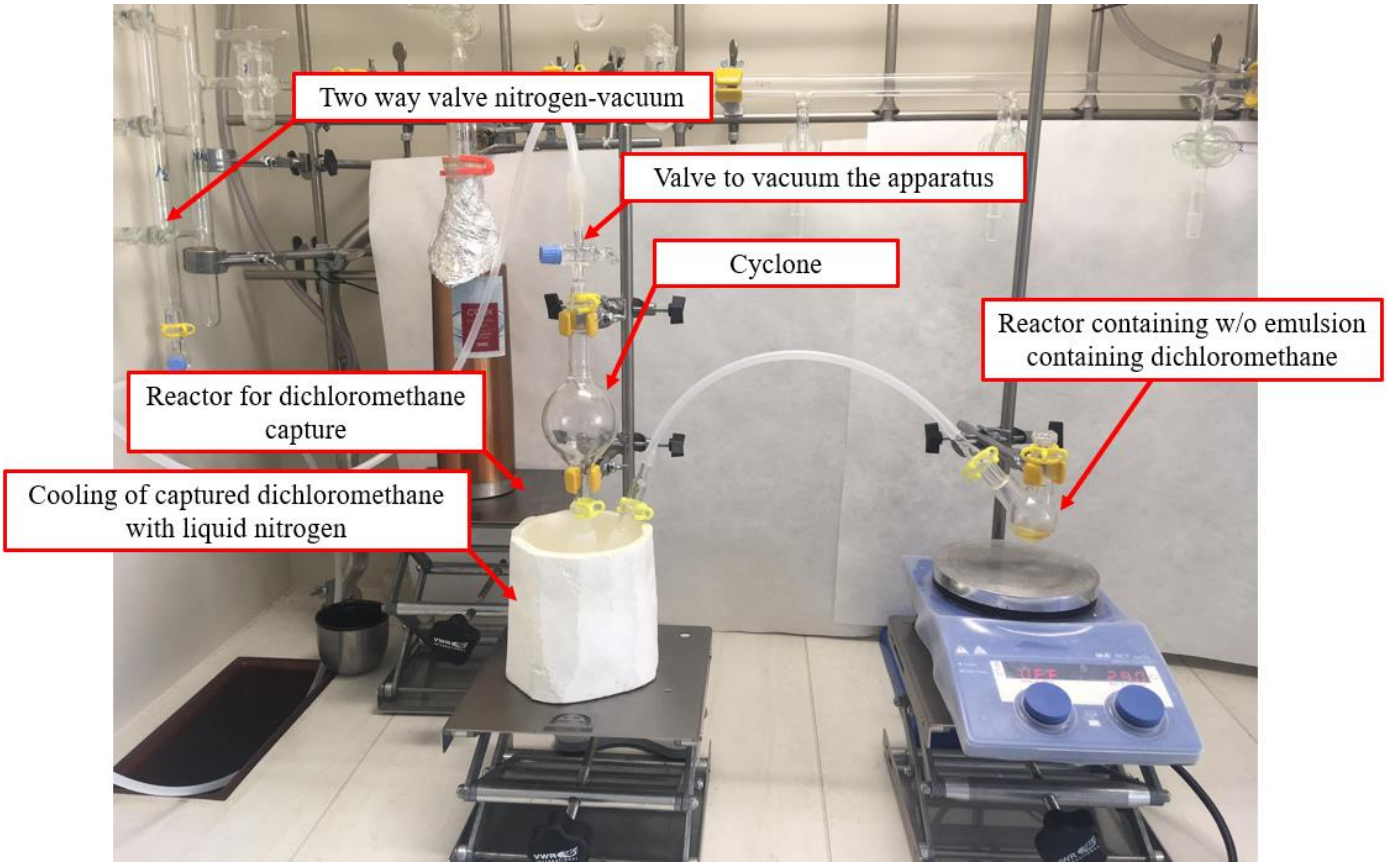

Figure 10 Vacuum line apparatus for dichloromethane evaporation

Finally, the liposome solution is then extruded through the 200 nm polycarbonate filter and then 10 times through a 100 nm polycarbonate membrane at 35 °C using the Avanti Mini-Extruder shown on Figure 11.

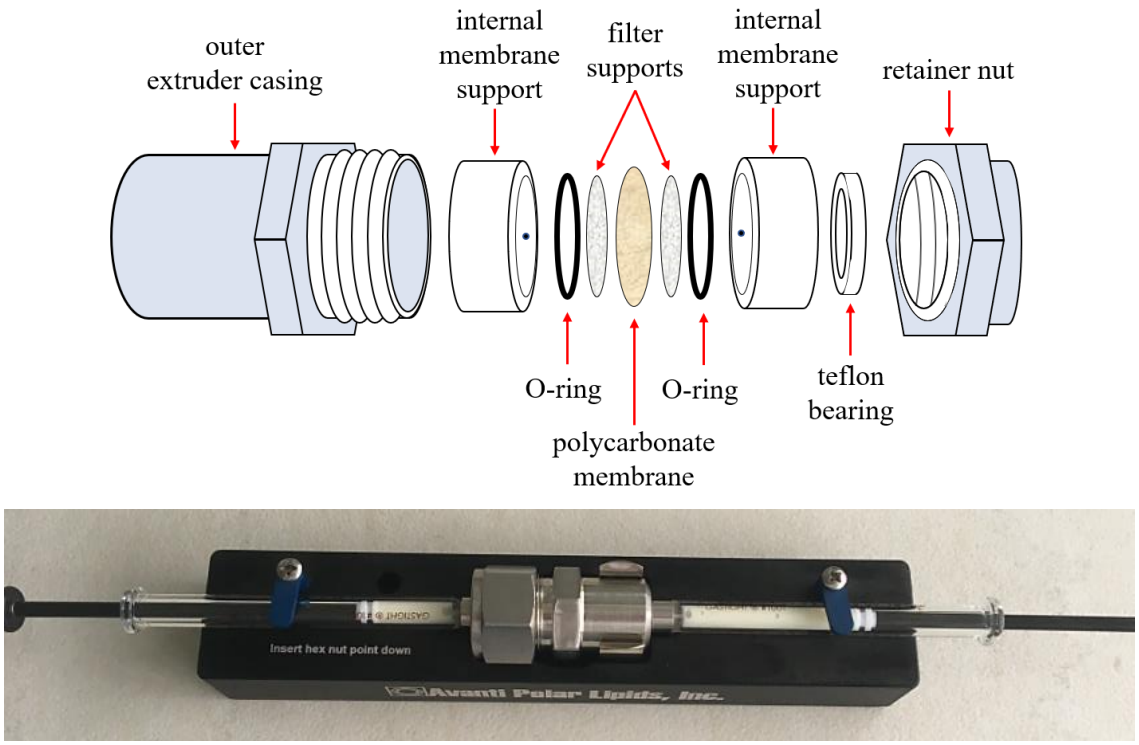

Figure 11 Avanti Mini-Extruder assembly scheme (up) and real-life Mini-Extruder during extrusion process (bottom)

4.4 Liposome characterization

Each prepared sample was subjected to a measurement of zeta potential and particle size distribution. FGF2-STAB® loaded samples were also tested for the encapsulation efficiency. After hydration and last sonication, samples were centrifuged at 4,200 rounds per minute for 30 minutes total using the Eppendorf Centrifuge 5804 R. The supernatant containing free FGF2-STAB® was collected and submitted to the encapsulation efficiency measurements. The free FGF2-STAB® has to be separated from the liposomes since it carries a charge on its own and affects the resulting charge. Sedimented liposomes were diluted with PBS 7.5 pH to reach the final volume of 2 ml and were submitted to zeta potential and size distribution measurements.

4.4.1 Stability measurements via zeta potential

The zeta potential was determined using the Zetasizer Nano ZS (Malvern, UK) at 25 °C using the 633 nm laser. The measurements were performed using glass cuvettes and a dip electrode by Malvern, UK. Each sample was always measured at least 5 times.

To determine the effect of pH on the zeta potential of liposomes, the liposome suspension was centrifuged at 4,200 rounds per minute (rpm) for 30 minutes using the Eppendorf Centrifuge 5804 R. The supernatant was collected, and the remaining liposomes were diluted with fresh PBS solution pH 7.5 to add up to a total volume of 2 ml. To test the pH dependence, a series of solutions in the range from pH 2 to pH 12 was prepared using PBS as a base and the pH was adjusted using 1 M KOH solution and 1 M H_3PO_4 solution. For each measurement, 100 µl of diluted liposomes were mixed to 1 ml of PBS with desiring pH and the solutions were measured using the Zetasizer Nano ZS.

4.4.2 Particle size and size distribution measurements

Particle size and particle size distribution were measured using the dynamic light scattering (DLS) detector (Wyatt Technology, Santa Barbara, USA) operating with a 658 nm laser at 25 °C while detecting scattering angle at 90°. Each measurement was done using the Wyatt Technology single-use DLS cuvettes containing a total amount of 4 µl of diluted liposome solution.

4.4.3 Encapsulation efficiency

To determine the encapsulation efficiency, the collected supernatant containing free nonencapsulated FGF2-STAB® was used. The supernatant was then qualitatively analysed using the Bradford protein assay using Bradford reagent which binds to protein molecules. This leads to the shift in their absorption maximum from 280 nm to 595 nm as displayed in Figure 11. Absorption measurements were performed on UV-VIS spectrophotometer V-730 (Jasco) by measuring the absorbance at 595 nm. Single cuvettes for UV-VIS spectrophotometry were used.

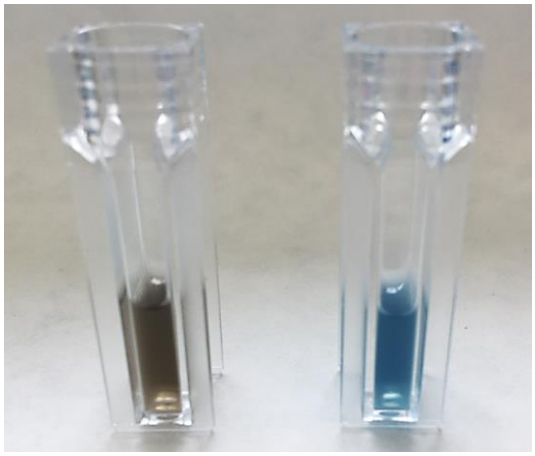

Figure 11 Left: unreacted Bradford reagent with brown staining, right: blue stained solution containing Bradford reagent after reagent-protein interaction occurred

The total amount of FGF2-STAB® present in each formula was calculated regarding the volume that was primarily pipetted into the formula. The concentrations of pipetted solution of FGF2-STAB® were 1 mg/ml and the initial volume of the formula being always 2 ml total.

Based on the expected entrapment efficiency being 60 %, the amount of FGF2-STAB® present in the supernatant of each formula was calculated and an adequate calibration and ratio of Bradford reagent to sample volume was used. By doing so, the concentration of nonencapsulated FGF2-STAB® present in the supernatant was calculated by using a calibration curve equation.

Bradford reagent to sample ratios and pipetted volumes are shown in Table 3, for most of the performed measurements, calibration for middle concentrations in the range from 10–100 µg/ml was used. The calibration curve and the equation are displayed on Figure 13.

Table 3 Reagent to sample volume to pipette for a single measurement and ratio of Bradford reagent to sample [78]

Calibration		Bradford reagent [ml]	Sample [ml]	Bradford reagent to sample ratio
Low concentration	1–10 µg/ml	0.50	0.50	1:1
Middle concentration	10–100 µg/ml	0.80	0.20	4:1
High concentration	100–1,000 µg/ml	1.00	0.03	33.3:1

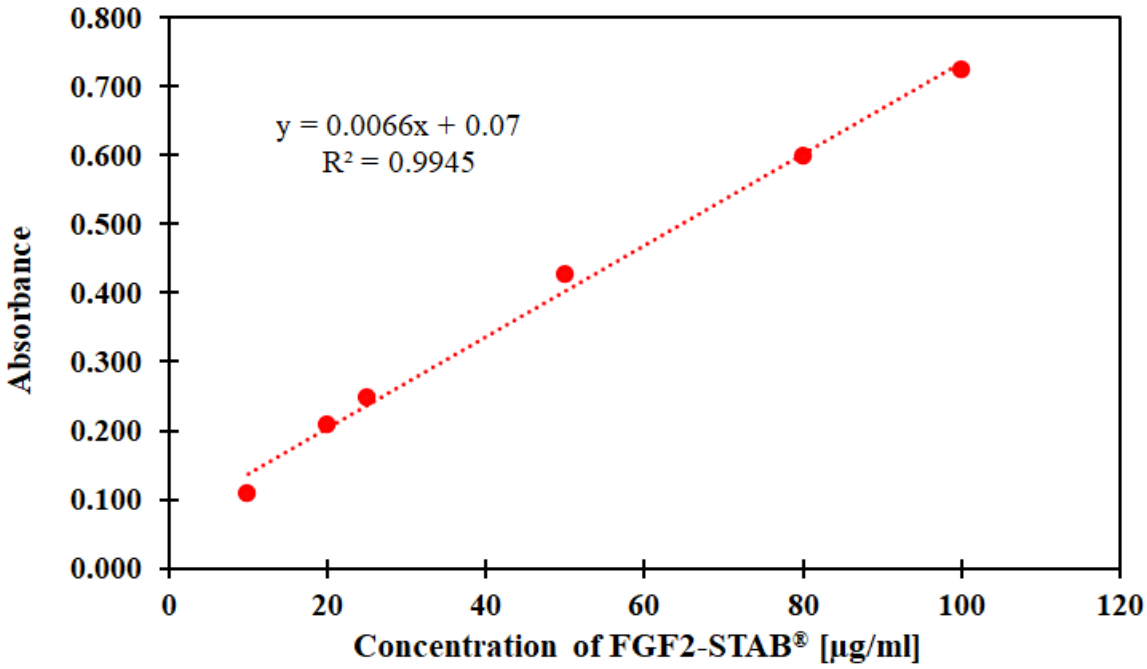

Figure 13 Calibration curve for middle concentrations of FGF2-STAB® to calculate free nonencapsulated protein in FGF2-LIP formula [78]

The encapsulation efficiency in percent was then calculated using the following equation [79]:

$$EE\ [\%] = \frac{(\text{FGF2-STAB}^{®}\ \text{in formula}) - (\text{FGF2-STAB}^{®}\ \text{in supernatant})}{(\text{FGF2-STAB}^{®}\ \text{in formula})} \times 100$$

4.4.4 Morphology of liposomes

Morphology of the empty LIP and the loaded FGF2-LIP was observed using the scanning transmission electron microscope MIRA3Raith (TESCAN). A drop of diluted liposome solution was placed on carbon-coated copper grids for electron microscopy and was left overnight to dry. These grids were viewed under STEM at suitable magnifications operating at an acceleration voltage of 20 kV at a working distance 5.68 mm.

Images were taken on samples after 7 days of storage since the day of preparation in the refrigerator at 4 °C.

5 RESULTS AND DISCUSSION

5.1 Liposome preparation optimization

The first attempts for liposome preparation of this thesis were based on the efforts of XU, He-Lin et. al [80] who succeeded in an effective encapsulation of FGF2 into liposomes used in silk fibroin-based hydrogels.

Samples were prepared according to [80], using the ratio of phosphatidylcholine (PC) to cholesterol (CHOL) ratio 10:1. In [80], PC and CHOL are co-dissolved in 5 ml of dichloromethane, then a volume of FGF2 solution is added to the mixture as a water phase. The mixture was further homogenized using probe sonication in ice water (10 s on, 10 s off, 20 s total) to obtain w/o emulsion. Afterwards, dichloromethane is removed from the emulsion by the rotary evaporator to form a lipid film. Residual dry lipid hydrogel was hydrated with 2 ml of pH 7.4 PBS at laboratory temperature for 12 h and further homogenized by sonication for 30 minutes (10 s on, 10 s off). Extrusion of liposomes through a polycarbonate membrane with 100 nm for 10 times pore size follows.

A common laboratory ultrasonic bath was used to substitute probe sonication. The water in the ultrasonic bath was cooled in advance using cooling gel bags until the temperature of water in the bath reached 3 °C. After each sonication, the temperature was measured, and water was cooled if needed. Because of a small amount of the w/o emulsion containing dichloromethane (5 ml), a rotary evaporator could not be used and therefore, a polymerization vacuum line was used to evaporate dichloromethane from the mixture. The setup for dichloromethane evaporation is displayed in Figure 10.

It was later discovered that the dichloromethane evaporation must be done precisely and all dichloromethane must be evaporated in this step. If it is not evaporated thoroughly and dichloromethane resides in the lipid after evaporation, the film cannot be hydrated sufficiently even after 18 hours of hydration and thus liposomes will not form afterwards during the second sonication.

5.1.1 Total mass of lipids 100 mg with 10:1 PC/CHOL ratio

In this step, the total mass of lipids was 100 mg, meaning 90.9 mg of PC and 9.0 mg of CHOL were used to prepare formulas 1–5 according to Table 4. Since empty liposomes were prepared first, the volume of FGF2-STAB® solution added was substituted with the same volume of PBS. The volume of PBS added was calculated following [80] where a solution of FGF2 with concentration 5 mg/ml was used.

Table 4 Formulas for liposome preparation with 10:1 ratio and 100 mg of total lipids

Formula	PC:PBS ratio	Theoretical loading of FGF2, 5 mg/ml [μg]	PBS solution added [μl]
1	1,000:1	100	20
2	500:1	200	40
3	300:1	300	60
4	250:1	400	80
5	200:1	500	100

Zeta potential (ZP) and diameter of the particles were measured and are displayed in Table 5, the particle size distribution (PSD) of *F1–5* is shown in Figure 14.

Table 5 Characterization of empty liposomes with different PBS solution load, formulas 1–5

Formula	PC/CHOL (100 mg total)	PBS solution added [μl]	Zeta potential [mV]	Particle diameter [nm]	
F1	10:1	20	2.33 ±3.28	–	132.1
F2	10:1	40	1.88 ±5.73	–	171.3
F3	10:1	60	-1.56 ±1.79	46.3	316.8
F4	10:1	80	0.02 ±6.03	–	186.3
F5	10:1	100	-7.93 ±6.37	–	161.8

The ZP of formulas 1–5 was in the range of ±30 mV. As a rule of thumb, particles with ZP around 0 mV within the ± 30 mV range are not considered as stable due to the fact that they are not repelling themselves and rather tend to attract one to each other. This suggests that the empty liposomes were not very stable in the system [81]. As Table 5 shows, the deviation of ZP in each formula is great. This indicates that the ZP changed drastically during each measurement and thus we could not propose these formulas as being stable.

What is also interesting is that particles of *F1*, *F2,* and *F4* carry an overall positive charge. Since liposomes are formed in aqueous environment, the polar heads of phosphatidylcholine in the lipid bilayer are faced into the aqueous solution. And since these polar heads carry a negative charge, the resulting liposomes should also carry a negative charge and thus exhibit a negative ZP. Moreover, particles with negative charge (negative ZP) are preferred for transdermal applications since these particles were shown to be cleared by the reticular endothelial system [82]. On the other hand, particles with positive ZP tend to absorb protein components in blood and thus have improved circulation half-life and due to charge interaction, are associated with cell destabilization, which is commonly used in targeting tumour cells [83, 84].

Most particles were within the distribution range of 132.1–186.3 nm, which is favoured in transdermal delivery and the distribution of these formulas was narrow (Figure 14). Only in the case of *F*3 containing 60 μl of PBS, a small number of particles had a smaller diameter around 46.3 nm and the major part of the particles with diameter bigger than the average, around 316.8 nm. Smallest particle diameters were obtained then with lowest PBS load of 20 μl, followed by the highest PBS load 100 μl, then the trend continued with particles loaded with 40 and 80 μl and the largest particles were obtained by using 60 μl of PBS.

Very narrow PSD was observed in *F4* as well as *F5,* with *F5* having the PSD curve shifted to smaller liposome diameters. Similar PSD curves were observed in *F1* and *F2,* with *F1* having the overall PSD curve shifted to smaller liposome diameters.

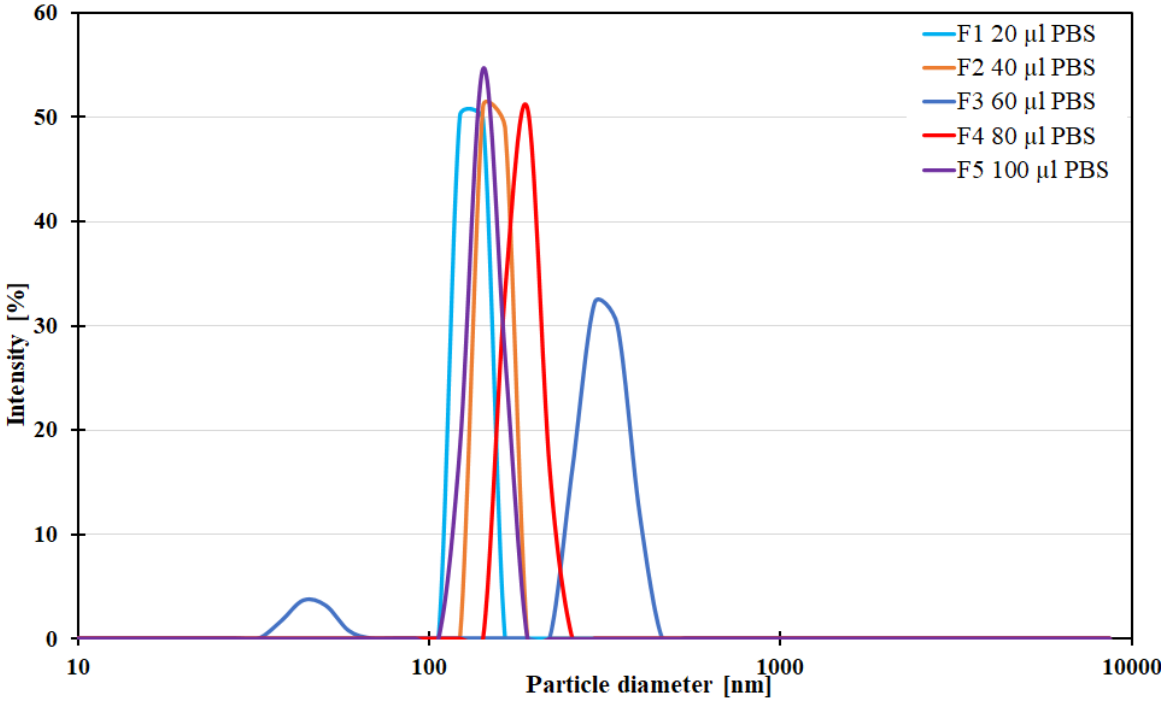

Figure 14 Particle size distribution and diameters of empty liposomes, F1–5

5.1.2 Total mass of lipids 110 mg with 10:1 PC/CHOL ratio

According to Arts et al. (1994) [85], ZP can be affected by the phosphatidylcholine content and the addition of PC can be effective for increasing ZP from about 10 mV to 60 mV but also that the ZP can be influenced by impurities. Therefore, liposomes with the same PBS loading and PC to CHOL ratio (10:1) were prepared but with increased total mass of lipids and therefore a higher PC content per formula. In formulas *F6–11*, the the mass of PC was 100.0 mg and mass of CHOL was 10.0 mg, giving a total mass of lipids 110.0 mg per formula. Since formula *F*5 prepared in 5.1.1 gave a very narrow distribution and relatively small diameter of liposomes, the load 200 µl of added PBS was also prepared to test whether the trend of lower diameters will continue with greater PBS volume. The PSD are shown in Figure 15 on the next page, ZP and particle diameter of formulas *F6–11* are displayed in Table 6.

Table 6 Characterization of empty liposomes with different PBS solution load, formulas 6–11

Formula	PC/CHOL (110 mg total)	PBS volume added [µl]	Zeta potential [mV]	Particle diameter [nm]	
F6	10:1	20	2.13 ±2.37	64.7	232.7
F7	10:1	40	3.60 ±2.37	–	168.3
F8	10:1	60	-3.45 ±8.73	–	203.2
F9	10:1	80	2.80 ±9.21	–	106.7
F10	10:1	100	-2.88 ±2.00	–	124.2
F11	10:1	200	2.51 ±0.99	–	159.5

ZP of liposomes *F6–11* was in the range from -3.45 to 3.60 mV, meaning that particles are not in the range of ZP of stable particles. Just like in previous formulas *F1–5*, the deviations of each measurement are too high and thus these liposomes cannot

be considered as stable particles. The only exception, where the ZP deviation was relatively small was *F11*, which is a formula containing 200 µl of PBS.

Liposomes of *F6–11* gave particles with diameter in the range from 106.7 to 232.7 nm, which is still considered as acceptable for transdermal delivery. Smallest diameter of 106.7 nm was obtained with *F9* (80 µl of PBS), followed by particles with diameter 124.2 nm given by *F10* (100 µl of PBS) and particles with diameter 159.5 nm given by *F11* (200 µl of PBS). Smaller volumes of PBS gave even larger diameters of liposomes.

Considering the PSD, the trend was similar as in the liposome diameter – the narrowest was of *F9*, followed by *F10* and *F11*. The measured intensity was also higher in the case of higher PBS volumes than when smaller PBS volumes were used – in *F6*, the maximum measured intensity was 23 %, but in *F9*, the intensity was 59 %. Except the liposomes *F6* containing 20 µl PBS, the higher content of lipids resulted in the formation of smaller liposome particles and the PSD curves became narrower. However, it was not confirmed that higher volumes of PBS result in smaller particles and narrower distribution, based on the *F11* results.

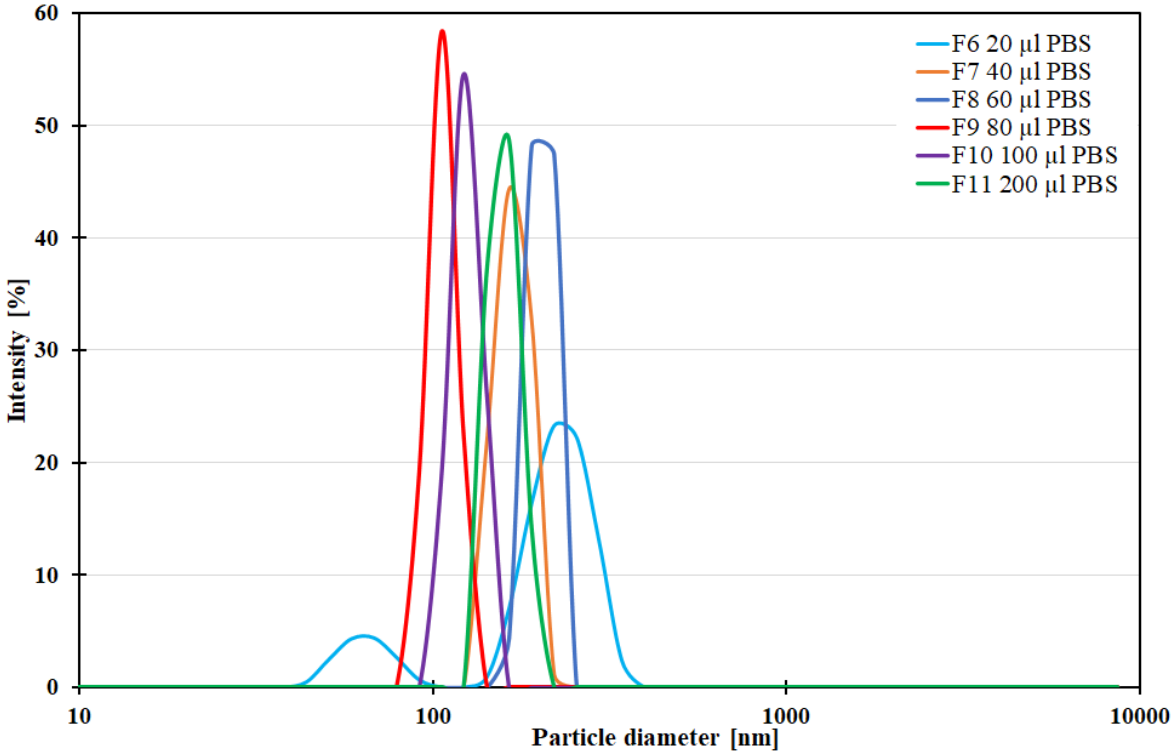

Figure 15 Particle size distribution and diameters of empty liposomes, F6–11

This indicates that the liposome size and PSD were affected by the volume of PBS in each formula and thus a "total lipid to liquid in formula" ratio must be considered (total lipids mean a sum of PC and CHOL). The dependence of the resulting liposome diameter of *F1–5* compared to *F6–11* on the volume of added PBS in the formulas is displayed in Figure 16; Table 7 compares the diameters of presented formulas based on the lipid to liquid ratio.

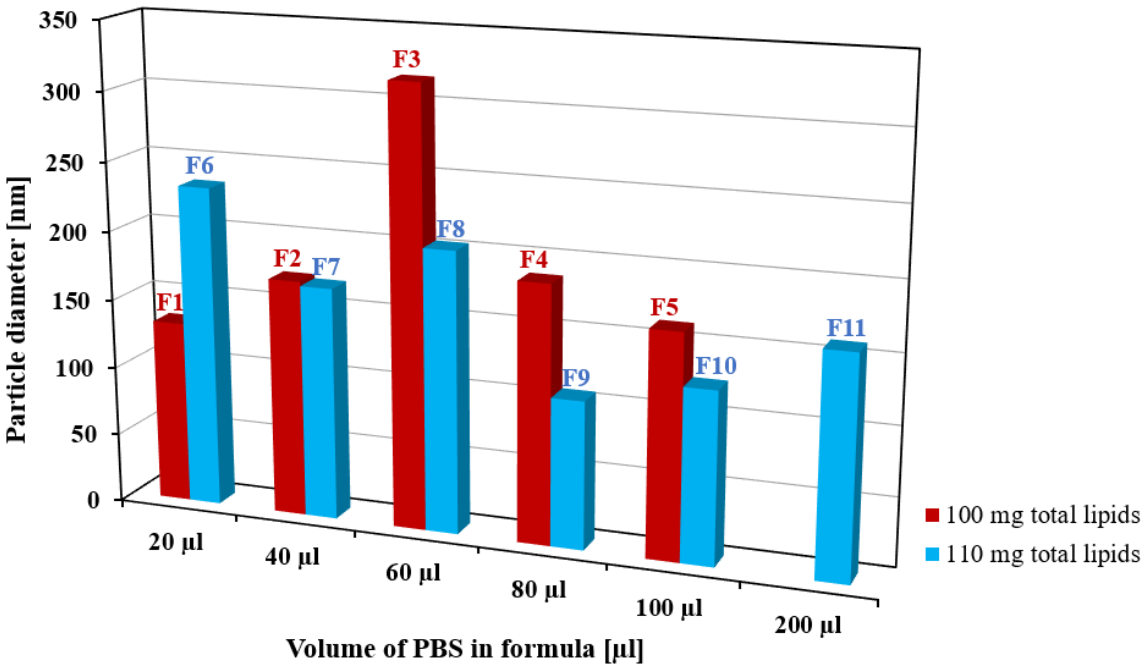

Figure 16 Dependence of particle diameter of F1–5 and F6–11 on the total added volume in formula

Table 7 Comparison of liposome diameters of F1–5 and F6–11 according to total lipid to liquid ratio in formula

Total liquid [µl]	Formulas *F1–5*				Formulas *F6–11*			
		Total lipids [mg]	Lipid/liquid ratio	Diameter [nm]		Total lipids [mg]	Lipid/liquid ratio	Diameter [nm]
20	1		5,000	132.1	6		5,500	232.7
40	2		2,500	171.3	7		2,750	168.3
60	3	100	1,667	316.8	8	110	1,833	203.2
80	4		1,250	186.3	9		1,375	106.7
100	5		1,000	161.8	10		1,100	124.2
200	–	–	–	–	11		550	159.5

As shown in Table 7 and on Figure 16, formulas *F6–11* containing higher lipid to liquid ratio give smaller liposome diameters (except *F6*) than when the lipid to liquid ratio is smaller as in the case of *F1–5*.

Going from *F6*, there was an increase in diameter of 76 % when compared to *F1*; the diameter decreased for 2 % in *F7* compared to *F2* and a decrease in diameter was also observed in *F8* for 36 % compared to *F3*. The most distinct decrease in diameter was when *F4* and *F9* are compared – by increasing the lipid/liquid ratio from 1,250 to 1,375, the liposome diameter decreased for 43 % in *F9*. Liposome diameter of *F10* decreased for 23 % when compared to *F5*.

It was shown that there is a correlation between particle diameter and total lipid to liquid ratio. By comparing *F1–5* and *F6–11*, there was a decrease in liposome diameter, and this decrease was the most significant in *F9* containing 110 mg of total lipids and 80 µl

of PBS. As displayed in Figure 17, there is almost a parabolic dependence of the decrease in diameter in *F1–5* and *F6–11* and the total added volume.

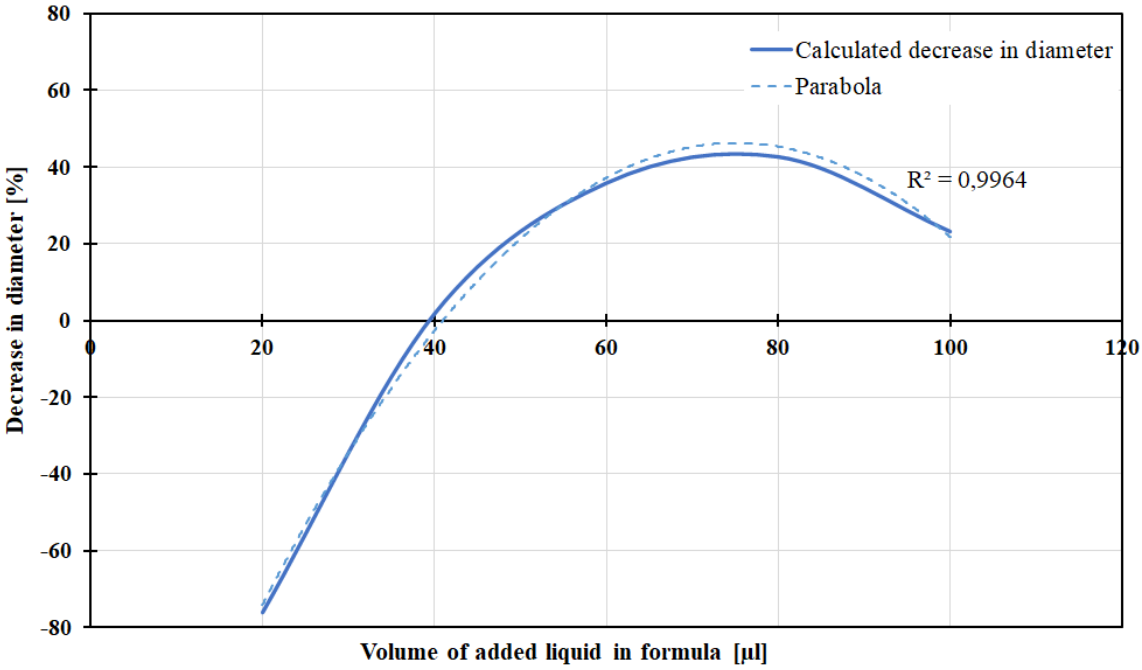

Figure 17 A decrease in diameter caused by the change in total lipid/liquid ratio with liquid content in formula

To achieve a narrower distribution and smaller liposomes, the formulas *F6–11* were further extruded ten times through a polycarbonate membrane with pore size 100 nm to obtain *F12–15, F17* and *F19*; and through a membrane with pore size 200 nm to obtain *F16* and *F18*. The results are displayed in Table 8.

Table 8 Characterization of extruded empty liposomes with different PBS solution load, formulas 12–19

Formula	PBS volume added [µl]	Extrusion	Zeta potential [mV]	Particle diameter [nm]		
12	20	10 × 100 nm	-7.69 ±0.94	8.3	424.6	–
13	40	10 × 100 nm	-8.71 ±2.10	7.4	376.9	–
14	60	10 × 100 nm	11.4 ±16.7	–	344.4	5,068
15	80	10 × 100 nm	-0.49 ±2.37	–	252.8	5,132
16	80	10 × 200 nm	-8.49 ±1.04	–	466.5	–
17	100	10 × 100 nm	-4.45 ±2.62	9.2	541.6	–
18	100	10 × 200 nm	-0.33 ±2.29	–	353.5	–
19	200	10 × 100 nm	-4.58 ±1.18	–	183.8	2,745

When compared to the corresponding formulas without extrusion, excluding *F14*, there was an improvement in the values and deviations of the ZP, but the values were still under the range between ±30 mV. This indicates that the ZP was more uniform during the measurements, but the stability of the system is still not sufficient. Except *F14*, all formulas from the group had negative ZP, which is beneficial for transdermal delivery. Good results regarding ZP measurements were obtained by *F12, F13,* and *F16*, where the

values of ZP were negative and the deviations were also small. As it was shown, there is also a difference in ZP between liposome formulas extruded through 100 nm and 200 nm polycarbonate membranes. *F15* extruded through a 100 nm pore size membrane carried an overall charge -0.5 ±2.4 mV, whereas *F16* extruded through a 200 nm pore size membrane carried an overall charge around -8.5 ±1.0 mV. Opposite situation occurred in *F18*, where there was an increase in ZP when the formula was extruded through a 200 nm pore size membrane from -4.45 ±2.6 mV in *F17* to -0.3 ±2.3 mV in *F18*. Moreover, formulas containing 100 µl (*F17*) and 200 µl (*F19*) of PBS gave similar results with ZP being around -4.5 mV.

On the other hand, as Figure 18 shows, liposome diameter increased in every extruded formula, liposomes in *F15–18* were more than twice as big as the original liposomes. In the case of *F16–F18*, the diameter of extruded particles increased by more than 300 % percent when compared to the original non-extruded particles. Good results show *F19*, where the increase of particle size between extruded and non-extruded samples increased by only 15 % but what must also be considered is the fact that in *F19*, as well as in *F14* and *F15*, particles with larger diameters around 3 and 5 µm were formed.

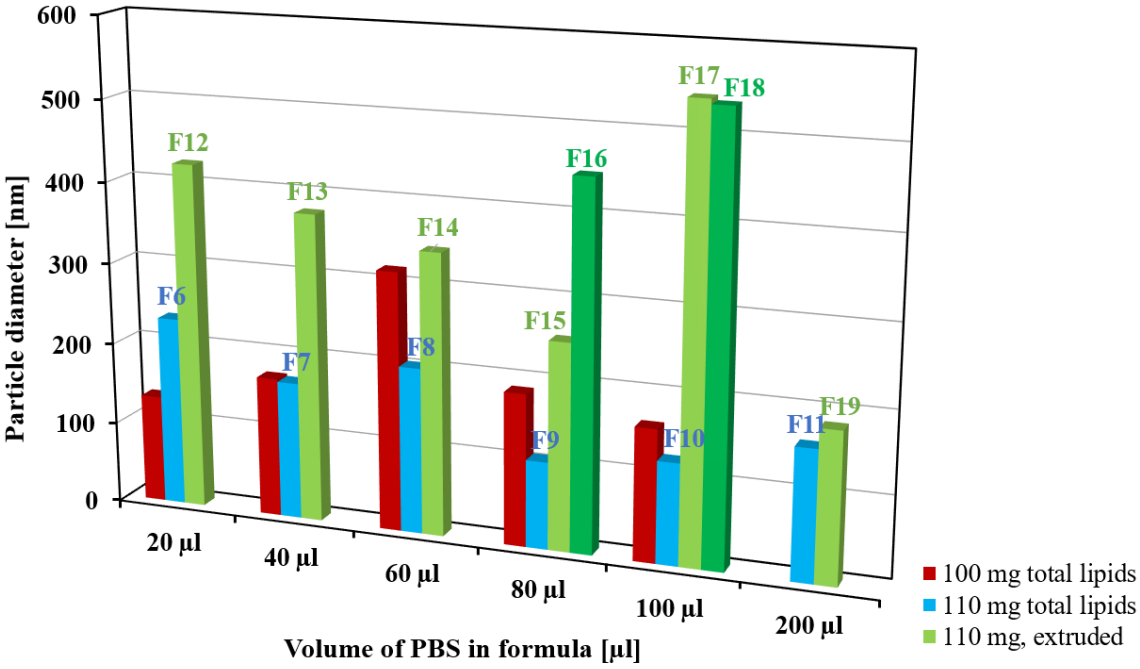

Figure 18 Dependence of particle diameter of F1–5, F6–11 and corresponding formulas extruded through polycarbonate membranes with pore size 100 nm (F12–F15, F17, F19) and 200 nm (F16, F18) on the total added volume in formula

Even though the particles were not stable, there is a trend in particle diameter. With the increased volume of PBS added, the diameter decreases from a load of 20 µl (424.6 nm) to 80 µl (252.8 nm) and then increases again at 100 µl of PBS (541.6 nm), considering the 10 × 100 nm extrusion. Of course, this is only for the case of the main particle size peaks. The formation of larger particles must be taken into count.

This enlargement of particle diameter could result from particle aggregation or agglomeration of smaller particles. If the particles have ZP values (small charge) within the ±30 mV range, there is no force to repel the particles and prevent their

flocculation and there can be a tendency to aggregate. [81]. During the particle agglomeration and/or liposome inclusion, it is possible that the entrapped liposome content is leaking into the liposome environment. To prevent agglomeration, negatively or positively charged lipids could be added into the liposome formulation to stabilize the liposomes.

This trend is very well displayed in Figure 19, where the width of PSD curves widen and do not become narrower as expected after extrusion. During extrusion, particles are pushed through a membrane with defined pore size under pressure, and this probably supports the agglomeration even more. In addition, the intensity measured by the Zeta-sizer is much smaller than in the previous non-extruded formulas.

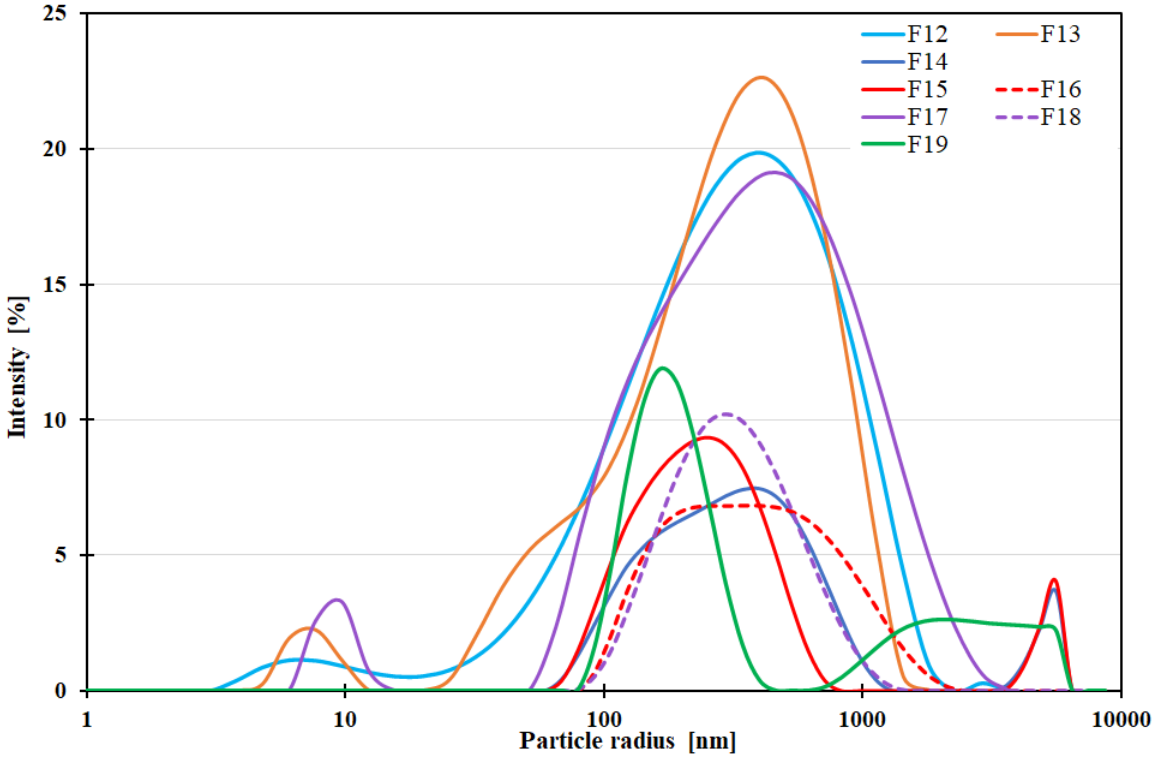

Figure 19 Particle size distribution of empty liposomes with corresponding F12–19, obtained by extrusion of F6–11 through 100 and 200 nm polycarbonate membranes

5.1.3 Phosphatidylcholine to cholesterol ratio

In previous formulas, it was shown that the mass of total lipids affects the zeta potential as well as the liposome size and size distribution. Because the purity of PC used in our experiments is only 60 % and the purity of PC used in [80] was 98 %, the mass of PC in our experiments was increased to match the purity of 98 %. Therefore, 163 mg of PC were used as the base for formulas *F20–23*. Since there will also be a higher cholesterol content in different formulas, this could result in stabilization of the system and in obtaining greater ZP values.

Even though the best results regarding the liposome diameter and size distribution from formulas *F1–11* were obtained by using a load of PBS 80 µl, regarding the zeta potential as the main stability factor, the best results were obtained by using a load of 100 µl of PBS. Formulas containing 100 µl of PBS (*F5* and *F10*) also gave satisfactory results

regarding the liposome diameter and PSD. Therefore, the following formulas *F20–25* were prepared using 100 μl of PBS. The results for *F20–23* are displayed in Table 9.

As shown in Table 9 bellow, there was a decrease in the ZP deviation value in *F23* (ratio 4:1), where the potential was -7.92 ±0.78 mV. When compared with previous formulas containing 100 μl of PBS, the ZP of *F5* was -7.93 ±6.37 mV and *F10* was -2.88 ±2.00. The value of ZP was similar to of *F5* but the deviation decreased and indicating that higher PC to CHOL ratio and higher total amount of PC influenced the system stability. However, the value of ZP still is not greater than ±30 mV. The data show a trend in ZP decrease with the increase of CHOL content and the total lipid amount in formula. On the opposite, spectra of ZP was *F20* with 10:1 PC/CHOL ratio, where ZP of 4.63 ±0.92 mV was achieved. When compared to the previously discussed *F5* and *F10* containing the same PC/CHOL ratio, there was an increase in ZP and a decrease in deviation with higher PC content. The *F21* containing 8:1 PC/CHOL ratio gave ZP of -0.97 ±3.34 mV and *F22* containing 6:1 PC/CHOL ratio gave ZP of -1.77 ±1.78 mV indicating that the particles produced by these formulas are not very stable and still would have tendencies for agglomeration.

Table 9 Characterization of empty liposomes with different PC/CHOL ratios, formulas 20–23, each formula containing 163 mg of PC and 100 μl of PBS

Formula	PC/CHOL	Total lipids [mg]	Zeta potential [mV]	Particle diameter [nm]		
20	10:1	179.3	4.63 ±0.92	15.8	189.6	–
21	8:1	183.4	-0.97 ±3.34	28.5	195.2	–
22	6:1	190.2	-1.77 ±1.78	5.2	251.5	–
23	4:1	203.8	-7.92 ±0.78	–	79.0	–

Particle size distribution is displayed in the next page on Figure 20. The particle diameter changed as well with the PC/CHOL ratio. The smallest diameter was reached in *F23*, where the diameter was determined at 79.0 nm and the distribution was unimodal, whereas in *F20–22*, the distribution was bimodal and smaller fractions between 5.2–28.5 nm was obtained. However, the smaller fractions do not represent an obstacle for transdermal drug delivery unlike bigger agglomerated particles larger than 200 nm. Formulas *F20* and *F21* were similar in particle size, the difference between these two formulas in size was only 5.6 nm. *F21* as a product of 8:1 PC/CHOL ratio contained larger particles with diameter 195.2 nm and a smaller fraction of 28.5 nm. *F20* formed by 10:1 PC/CHOL ratio contained particles of 189.6 nm in diameter and a smaller fraction of particles with diameter 15.8 nm. Largest particles of *F20–F23* gave *F22* formed by 6:1 PC/CHOL ratio and contained particles of 251.5 nm in diameter and a smaller fraction of particles with diameter 5.2 nm.

Interesting results gave *F20* containing 10:1 PC/CHOL ratio and an amount of 163 mg PC, having particle diameter 189.6 nm, but corresponding formulas with 10:1 PC/CHOL ratio gave 161.8 nm (*F5*; 90.9 mg PC) and 124.2 nm (*F10*; 100 mg PC). Even though there was a decrease in particle size of 37.6 nm going from 90.9 mg of PC to 100 mg of PC, there was a raise of 65.4 nm with another increase of 63 mg of PC. This could mean that there is a maximum of possible PC content per 100 μl of liquid, in this case 100 μl of PBS.

From the following Figure 20, it is evident that *F23* gave not only the smallest particles in size but also the narrowest PSD curve from the group of *F20–F23*. The difference in intensity between the groups is noticeable, *F23* reaching the intensity of 81 %, *F20* and *F21* reaching a similar intensity of 33 %, whereas *F22* reached the intensity maximum at 13 %.

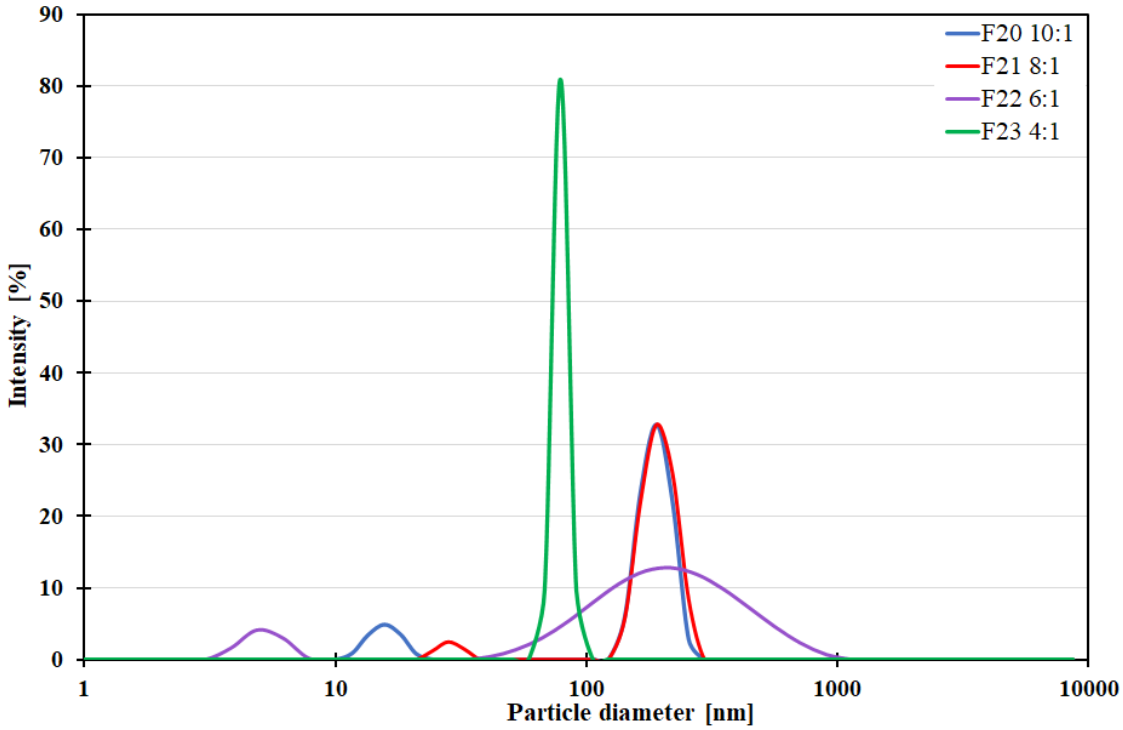

Figure 20 Particle size distribution and diameters of empty liposomes, F20–23

F20 and *F21* not only contained particles with similar diameter, but also the width of their PSD curves was similar. They also shared a similar intensity of 33 %. The width and shape of the size distribution curve of *F22* indicates that the liposome solution did not contain liposomes of similar diameter but rather liposomes of various diameters with the diameter maximum at 251.5 nm. Even though *F22* with ratio 6:1 gave the largest diameters of particles in the main fraction, the particles in the smaller fraction were much smaller in diameter than in the formulas formed with PC/CHOL ratios 8:1 and 10:1.

The reason that the main fraction of particles of *F20–22* than *F23* had larger diameters might be that the smaller particles have some influence on the larger particles. It could be possible that the majority of particles from *F20–22* form a narrower size distribution curve, but due to the agglomeration of the smaller fractions with a small charge (zeta potential), the diameter of particles detected is increased and this results in particles with bigger diameters and wider size distribution curves.

Discussed formulas *F20–23* were also extruded to give formulas *F20e–23e*, these were extruded through polycarbonate membranes with 200 nm pores once and then through a filter with 100 nm pore size ten times at 35 °C. Zeta potential and particle diameters of *F20e–23e* are displayed in Table 10.

Table 10 Characterization of empty liposomes with different PC/CHOL ratios, formulas 20e–23e, each formula containing 163 mg of PC and 100 µl of PBS, extrusion 1 × 200 nm and then 10 × 100 nm filter

Formula	PC/CHOL	Total lipids [mg]	Zeta potential [mV]	Particle diameter [nm]		
20e	10:1	179.3	-2.49 ±5.20	–	349.7	5,380
21e	8:1	183.4	-0.75 ±3.87	74.8	418.4	5,398
22e	6:1	190.2	0.78 ±0.64	54.8	286.4	5,727
23e	4:1	203.8	-4.13 ±0.56	–	159.7	–

By performing an extrusion of *F20* to obtain *F20e*, there was a decrease in the overall charge from 4.6 ±0.9 mV in *F20* to -2.49 ±5.2 mV in *F20e*, but also an increase in deviation was noticed indicating that the system overall charge differed during the performed measurements. Formulas *F21* and *F21e* gave similar ZP as well as its deviations and the charge was not affected by the performed extrusion. When ZP of *F22* and *F22e*, is compared, in *F22e* there is an increase of ZP going from -1.8 mV ±1.8 mV in *F22* to 0.8 ±0.6 mV in *F22e* but the deviation of ZP decreased. Increase in ZP was also detected in *F23e*, going from -7.9 ±0.78 mV in *F23* to -4.1 ±0.6 mV in *F23e*.

The overall changes in ZP when non-extruded and extruded formulas are compared rose gradually with higher cholesterol content (smaller PC/CHOL ratio) in the formulas as displayed on Figure 21.

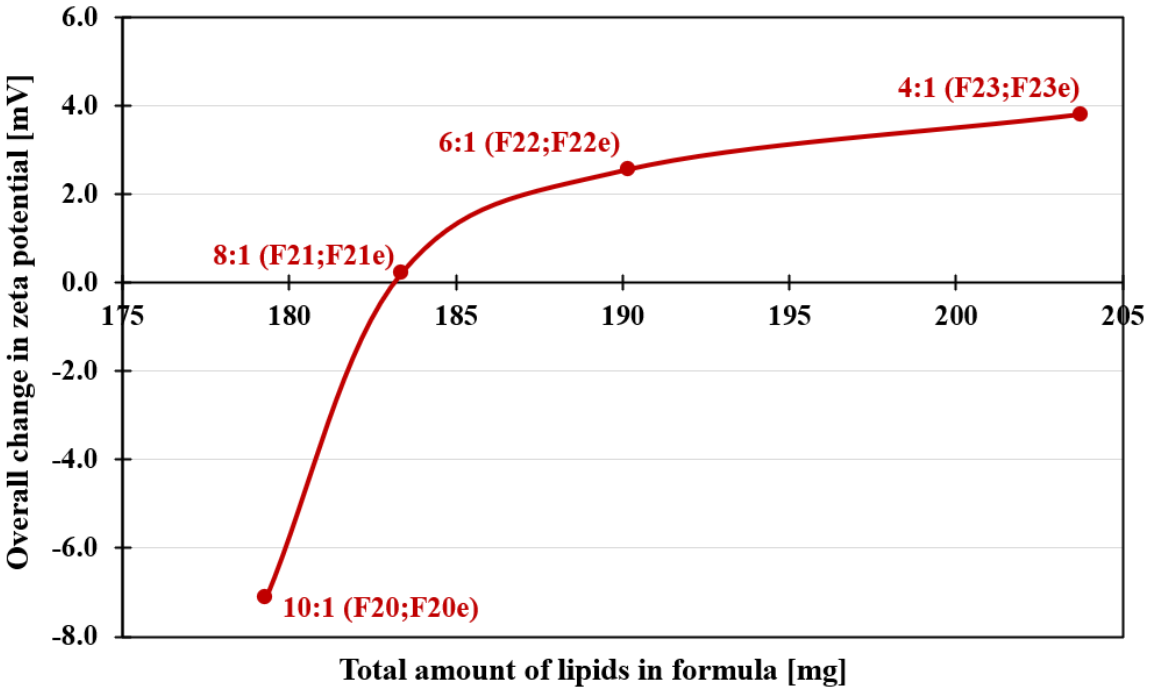

Figure 21 Comparison of the overall change in ZP in non-extruded and extruded formulas F20–23 and F20e–F23e

Following Figure 22 shows the comparison of PSD curves of the corresponding extruded and non-extruded formulas, the liposome diameters were shown in the previous Table 10. In all extruded formulas, a rise in liposome diameter was detected. Furthermore, in *F20–22*, larger diameters of liposomes were obtained, in the case of *F22* liposomes with

diameter around 600 nm were formed, but in the case of *F20* and *F21*, larger particles around 5.4 µm were formed and thus are not beneficial or could be even harmful in transdermal drug delivery. Even though there was a rise in liposome diameter in *F23e* compared to *F23*, the PSD curve width of extruded liposomes is similar to the PSD curve of non-extruded liposomes, but the intensity of scattered light decreased from 81 % to 52 %. In the remaining formulas *F20–F22*, there was a decrease in intensity when DLS was measured, and the PSD curves shifted to larger diameters and fractions with larger diameters were formed.

In conclusion, regarding the measured parameters (ZP, liposome diameter, and PSD curves), the best results were obtained by use of *F23* containing 4:1 PC/CHOL ratio and corresponding extruded formula *F23e* when compared to other formulas in the group.

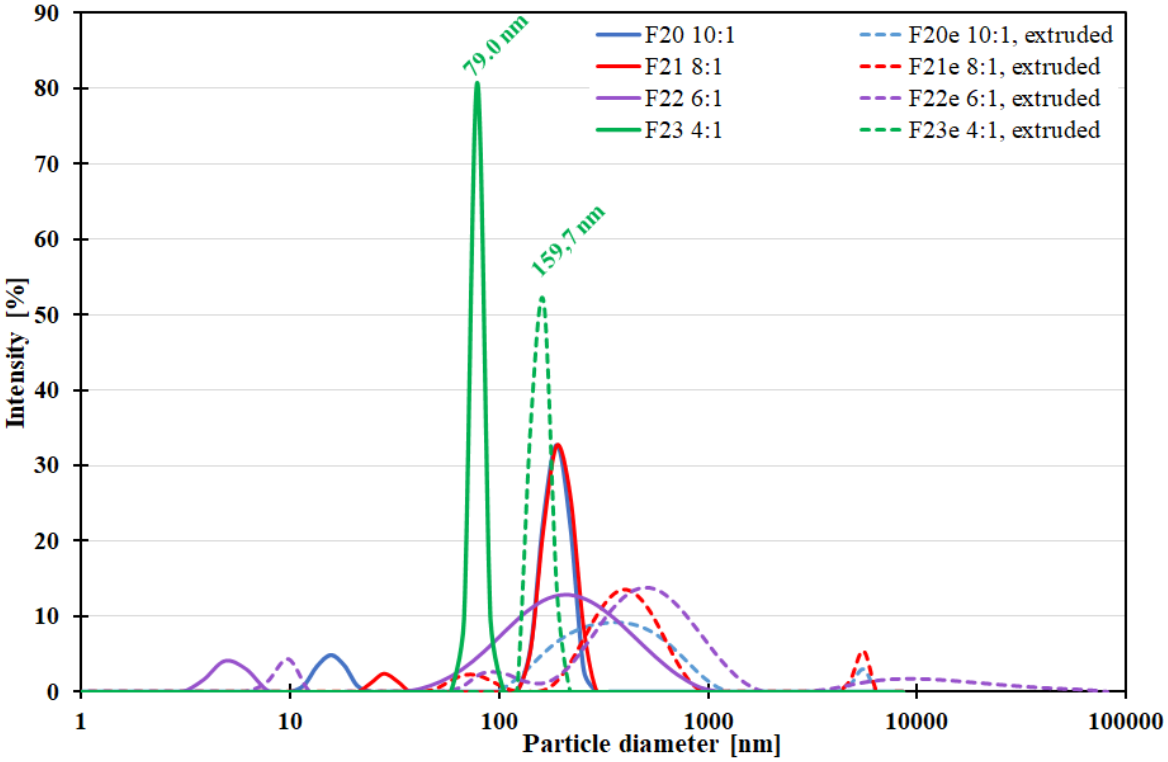

Figure 22 Particle size distribution of empty liposomes F20–23 and corresponding extruded liposomes F20e–23e

Considering these results, this could mean that there is a maximum of possible PC content per 100 µl of liquid, in this case 100 µl of PBS. To test this theory, formulas *F24–27* containing smaller PC and therefore also a CHOL content with total amount of lipids 150 mg were prepared. Results for these formulas are displayed in Table 11.

Table 11 Characterization of empty liposomes with different PC/CHOL ratios, formulas 24–27, each formula containing 150 mg of PC and 100 µl of PBS

Formula	PC/CHOL	Total lipids [mg]	Zeta potential [mV]	Particle diameter [nm]		
24	10:1	179.3	0.61 ±2.16	58.3	451.6	–
25	8:1	183.4	-3.91 ±5.12	18.6	237.8	–
26	6:1	190.2	6.15 ±3.43	30.8	238.0	–
27	4:1	203.8	-4.05 ±2.93	3.1	421.8	–

As Table 11 shows, there is no correlation between the PC/CHOL ratio (or total amount of lipids) with ZP; measured ZP values also had great deviations. Moreover, when comparing *F20–23* and *F24–27*, it is obvious that better ZP results were obtained by using higher lipid content regarding the ZP (overall charge of liposomes) and its deviations.
Comparing the liposome diameter of *F20–23* and *F24–27*, the smaller amount of total lipids resulted in smaller particle diameters of particles in *F26*, where a decrease in diameter of 13.5 nm went from 251.5 nm in *F22* to 238.0 nm in *F26*. Relatively good results brought *F25* with liposome diameter 237.8 nm and a narrow PSD curve (Figure 23), similar liposome diameters were given by *F26* discussed earlier, but the PSD curve was not very narrow and the maximal intensity of scattered light from DLS was lower than in the case of *F25*. Similar PSD curve shape and intensity of DLS was obtained by *F27* containing 4:1 PC/CHOL ratio, but the overall diameter of liposomes was shifted to 421.8 nm. Similar diameter of liposomes was in *F24*, where the diameter was 541.6 nm in the main fraction, but the overall PSD curve width was bigger and the intensity of DLS smaller. In each formula from this group, *F24–F27*, a small fraction of liposomes with smaller diameters in the range from 3.1–58.3 nm was formed and could result in further agglomeration.

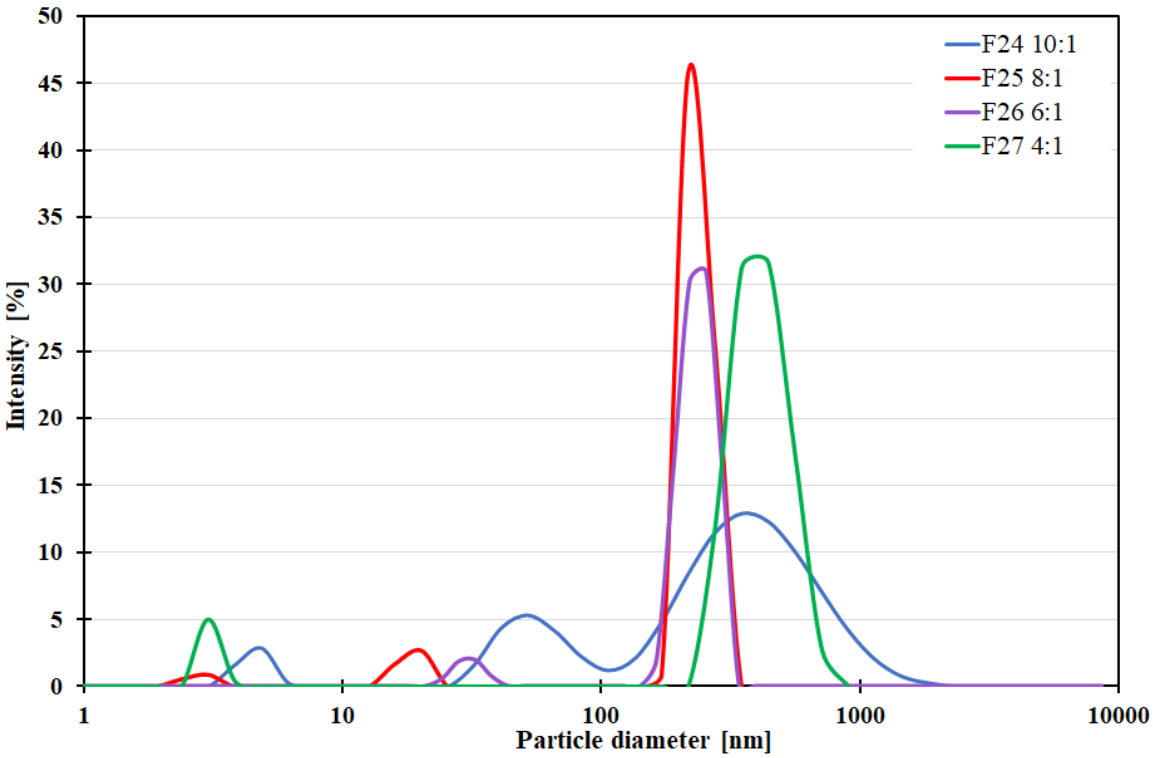

Figure 23 Particle size distribution and diameters of empty liposomes, F24–27

Discussed formulas *F24–27* were also extruded to give formulas *F24e–27e*, these were extruded again through polycarbonate membranes with 200 nm pores once and then through a filter with 100 nm pore size ten times at 35 °C. Zeta potential and particle diameters of *F24e–27e* are displayed in Table 12.

Table 12 Characterization of empty liposomes with different PC/CHOL ratios, formulas 24e–27e, each formula containing 150 mg of PC and 100 µl of PBS, extrusion 1 × 200 nm and then 10 × 100 nm filter

Formula	PC/CHOL	Total lipids [mg]	Zeta potential [mV]	Particle diameter [nm]		
24e	10:1	179.3	1.17 ±0.64	4.3	406.2	–
25e	8:1	183.4	5.98 ±2.06	4.0	664.1	3310
26e	6:1	190.2	7.28 ±2.70	3.3	717.5	–
27e	4:1	203.8	-6.96 ±2.73	7.0	741.5	–

After extrusion, there was an increase in ZP in *F24e–26e* compared to the corresponding *F24–26*, in the case of *F27e* there was a decrease in ZP compared to *F27*. However, in all presented formulas *F24e–27e*, there was an improvement in ZP deviation. An overall change in ZP of *F24e–27e* compared to *F24–27* did not correlate with total amount of lipids in the formula as it has in *F20–23* compared with *F20e–23e*. Following Figure 24 compares PSD curves of extruded *F24e–27e* and non-extruded formulas *F24–27*.

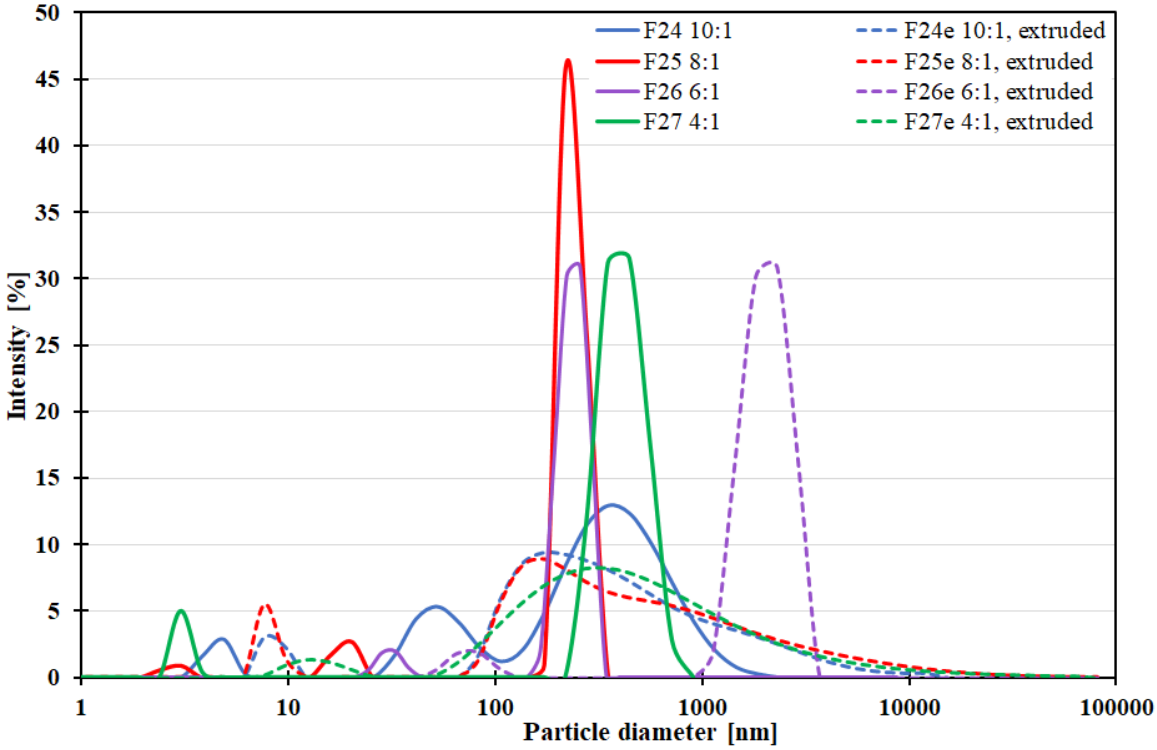

Figure 24 Particle size distribution of empty liposomes, F24–25 and corresponding extruded liposomes F24e–27e

Looking at the PSD curves, it is obvious that the liposome diameters were in a large range of diameters and thus the particle diameters displayed in Table 12 represent the diameter that most of the liposomes had. In each formula, the intensity of the detected scattered light decreased, and the width of PSD curves has widened. In *F27e*, a fraction

of liposomes with a diameter around 3.3 μm was formed and represents the fraction of the highest measured intensity and the narrowest curve in the PSD of this formula. In conclusion, decrease of total lipids in the formulas did not result in smaller liposome diameters, smaller ZP, or narrowing in the PSD curves.

5.2 Effect of pH on zeta potential

Apart from the temperature and purity of used materials, ZP can be also drastically affected by pH in aqueous media. Based on the results in 5.1.3, formulas *F20–23* were prepared to test the dependence of ZP on pH of the environment. For these measurements, formulas *F20–23* were prepared according to 4.4.1 and their ZP was measured. Table 13 shows the measured potentials of *F20–23* in an environment with varying pH compared to previously measured ZP.

Table 13 Zeta potential of F20–23 with increasing pH of the environment, each formula containing a volume of 100 μl of PBS

pH	Zeta potential [mV]			
	F20	F21	F22	F23
2	5.80 ±0.98	3.26 ±1.13	2.74 ±1.20	1.66 ±0.60
3	-3.87 ±0.37	-6.76 ±1.41	-4.73 ±1.11	-4.81 ±1.22
4	-7.35 ±0.94	-10.54 ±0.38	-5.61 ±1.53	-5.18 ±1.24
5	-12.92 ±0.92	-11.84 ±0.46	-10.19 ±1.11	-5.79 ±0.79
6	-18.42 ±2.11	-12.53 ±1.85	-11.76 ±0.58	-6.79 ±0.91
7	-20.10 ±2.15	-12.90 ±2.43	-12.92 ±1.63	-13.34 ±0.63
8	-20.86 ±2.45	-13.62 ±2.41	-12.72 ±1.52	-16.34 ±1.18
9	-26.02 ±0.95	-15.22 ±1.86	-14.08 ±2.05	-17.88 ±3.57
10	-26.80 ±0.64	-15.30 ±2.28	-14.16 ±2.25	-18.94 ±1.35
11	-36.56 ±0.58	-15.74 ±0.71	-18.38 ±2.60	-20.62 ±0.95
12	-39.56 ±0.82	-24.82 ±0.90	-23.28 ±1.69	-22.72 ±1.10

Measurements have shown that the ZP is significantly influenced by pH of the environment. ZP of each of these formulas decreased with increasing pH. The deviation of measured ZP also decreased, meaning that in a more acidic environment from pH 2 to pH 5, the overall charge of liposomes was more uniform. This trend is also visible in *F20*, where small ZP deviations were obtained also in basic pH from pH 9 to pH 12.

It was discovered that measured formulas displayed an overall negative charge in neutral pH 7, which is beneficial for transdermal drug delivery systems. *F21–23* gave ZP from -12.90 to -13.34 mV with relatively small deviations, whereas *F20* gave a much smaller ZP of -20.10 mV.

Considering the value of ZP of -30 mV as a line between stable and nonstable colloid nanoparticles, only liposomes of *F20* have reached the boundary of -30 mV and reached even ZP of -39.56 mV. Other formulas reached the smallest ZP only in the range of -22.72 to -24.82 mV and did not comply with the stable colloid particles boundary.

Since ZP of *F20–23* did not reach the positive value of + 30 mV in the measured range of pH of the environment, it is possible that this ZP would be measured at lower pH. Moreover, the ZP of *F21–23* did not reach the opposite side of ZP value - 30 mV in the

measured range of pH of the environment, but it is possible that the ZP around the -30 mV would be reached at higher pH. In either case, pH smaller or higher than around the values between pH 7 and pH 8 is not acceptable for intended *in vivo* applications of the prepared liposomes and would not be gentle if liposomes were loaded with proteins.

The dependence of measured ZP values on pH of the presented formulas *F20–23* is shown in Figure 25. By observing the decreasing curves of ZP with increasing pH, the isoelectric points of the formulas were assessed. The isoelectric point of *F20* was evaluated at pH 2.60, of *F21* and *F22* at pH 2.4, and of *F23* at pH 2.3.

In conclusion, the best results of ZP dependence on pH of the environment were given by the formula *F20* containing 10:1 PC/CHOL ratio, prepared with 163 mg of PC, 16.3 mg and CHOL and 100 µl of PBS.

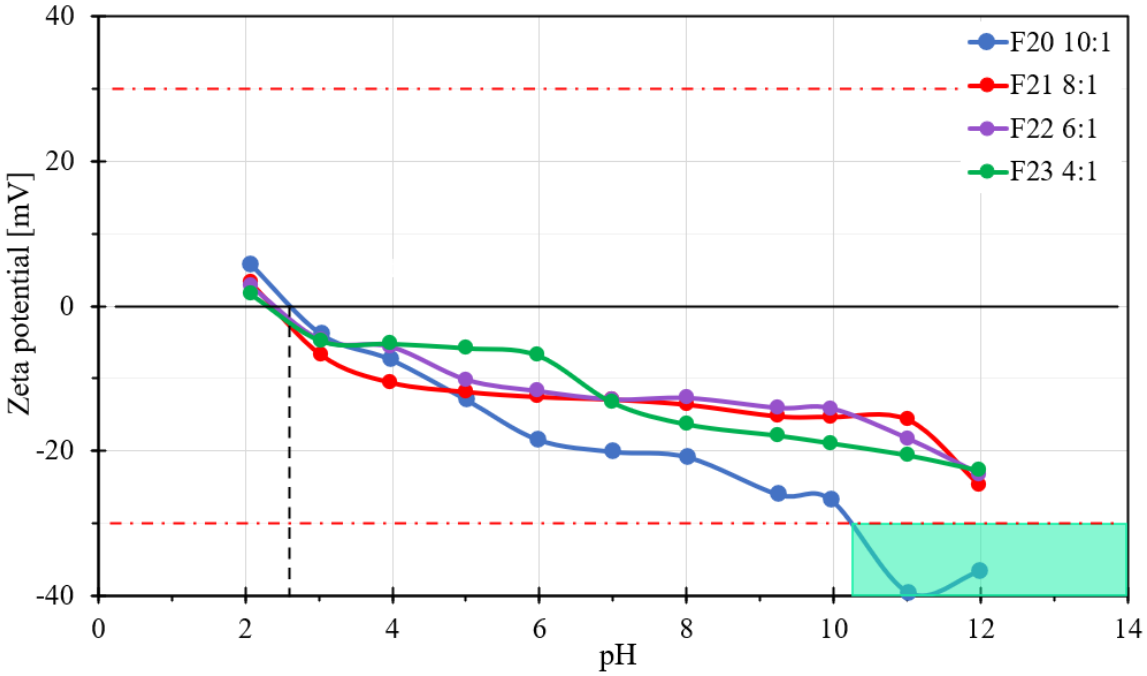

Figure 25 Dependence of zeta potential of formulas F20–23 on pH of the environment

5.3 FGF2 loaded liposome (FGF2-LIP) preparation

Based on result 5.1.3, the best results were given by using 4:1 PC/CHOL ratio represented by formulas *F23* and *F23e*. Even though the results in 5.2 have shown that it is not possible to reach the ZP smaller than -30 mV in the range of pH 7.5, the measured ZP and its deviations were satisfactory and of the same sort as *F21* or *F22*. Therefore, the following formulas were prepared using the same PC content of 163 mg and CHOL content of 40.8 mg and the same preparation technique. Formulas *F28–32* were prepared by using a defined volume of FGF2 solution with concentration 1 mg/ml to create a series with a changing PC/FGF2 ratio according to Table 14.

Table 14 Preparation of FGF2 loaded liposomes with different PC/FGF2 ratios, formulas F28–32 containing 163 mg of PC and PC/CHOL ratio 4:1

Formula	PC/FGF2	FGF2 load [mg]	FGF2 concentration in formula [μg/ml]
28	2,000:1	82	40.8
29	1,500:1	109	54.3
30	1,000:1	163	81.5
31	500:1	326	163.0
32	300:1	543	271.7

5.4 Characterisation of FGF2-LIP

The resulting zeta potential, particle diameter, and encapsulation efficiency of *F28–32* are displayed in Table 15.

Table 15 Characterization FGF2-LIP with varying PC/FGF2 ratios, formulas F28–32 containing 163 mg of PC and PC/CHOL ratio 4:1

Formula	PC/FGF2	Zeta potential [mV]	Particle diameter [nm]			EE [%]
28	2,000:1	1.00 ±1.70	9.7	976.1	–	12.0
29	1,500:1	-10.63 ±2.15	5.3	759.6	–	6.5
30	1,000:1	-4.42 ±4.80	7.0	104.7	–	14.9
31	500:1	-2.01 ±1.14	5.3	519.6	–	3.8
32	300:1	0.89 ±1.31	14.4	606.3	5,470	7.2

5.4.1 Stability measurements via zeta potential

In formulas *F28–32*, the encapsulated growth factor FGF2-STAB® can influence the system stability due to the implication of hydrogen bonding via protein-liposome and protein-protein interactions. *F23* containing the same ratio of PC/CHOL gave the ZP -7.92 ±0.78 mV. As seen in Table 15, ZP was significantly affected by the encapsulated FGF2-STAB® since the ZP deviations are relatively large. *F28* with the highest PC/FGF2 ratio gave a positive ZP of 1.00 ±1.70 mV, followed by *F32* with the smallest PC/FGF2 ratio with ZP of 0.89 ±1.31 mV. Going from PC/FGF2 ratio 1,500:1, the ZP increased with decreasing PC/FGF2 ratio. Since each formula contains liposomes with smaller diameters, there is a risk of aggregation and agglomeration of these particles.

5.4.2 Particle size and size distribution measurements

As displayed in Table 15 and on Figure 26, all prepared formulas formed a fraction of smaller particles in the range from 5.3 to 14.4 nm. Going from the smallest FGF2-STAB® content, *F28* formed a smaller fraction of particles with diameter 9.7 nm and most of the particles had a diameter around 976.1 nm. This diameter is the largest and the size distribution curve has the largest width of all prepared formulas *F28–32*. *F29* containing the ratio PC/FGF2 1,500:1 has formed most of the particles with diameter 759.6 nm and a smaller fraction with diameter 5.3. In addition, the *F29* does not only have a very narrow size distribution curve but also reaches relatively high intensity. Particles around 104.7 nm were formed in *F30* and a smaller fraction of liposomes with diameter around 7.0 nm was present, meaning that liposomes present in *F30* had the smallest diameter in this group. *F31* gave liposomes with diameter standing at

519.6 nm for most particles and at 5.3 nm for the smaller fraction. The distribution curve of *F31* is well defined but not as narrow as of *F29* or *F30*. Formula *F32* formed particles with large diameter around 5.5 µm, with diameters 606.3 nm and a smaller fraction of particles with small diameter around 14.4 nm. Even though *F32* forms relatively large particles, the peak on the distribution curve is well defined as well as the peak at 606.3 nm, which is much narrower than that of *F31*.

In conclusion, formula *F30* gave satisfying results regarding the requirement of forming liposomes with diameter around 100 nm and a narrow size distribution and would be good for transdermal FGF2-STAB® delivery. Liposomes formed by *F28* and *F30–32* would probably retain only at the top layers of the epidermis and would not be able to penetrate into the deeper layers of the skin in neither of the routes mentioned in 2.2 and the therapeutic effect of FGF2 on fibroblasts would not be reached.

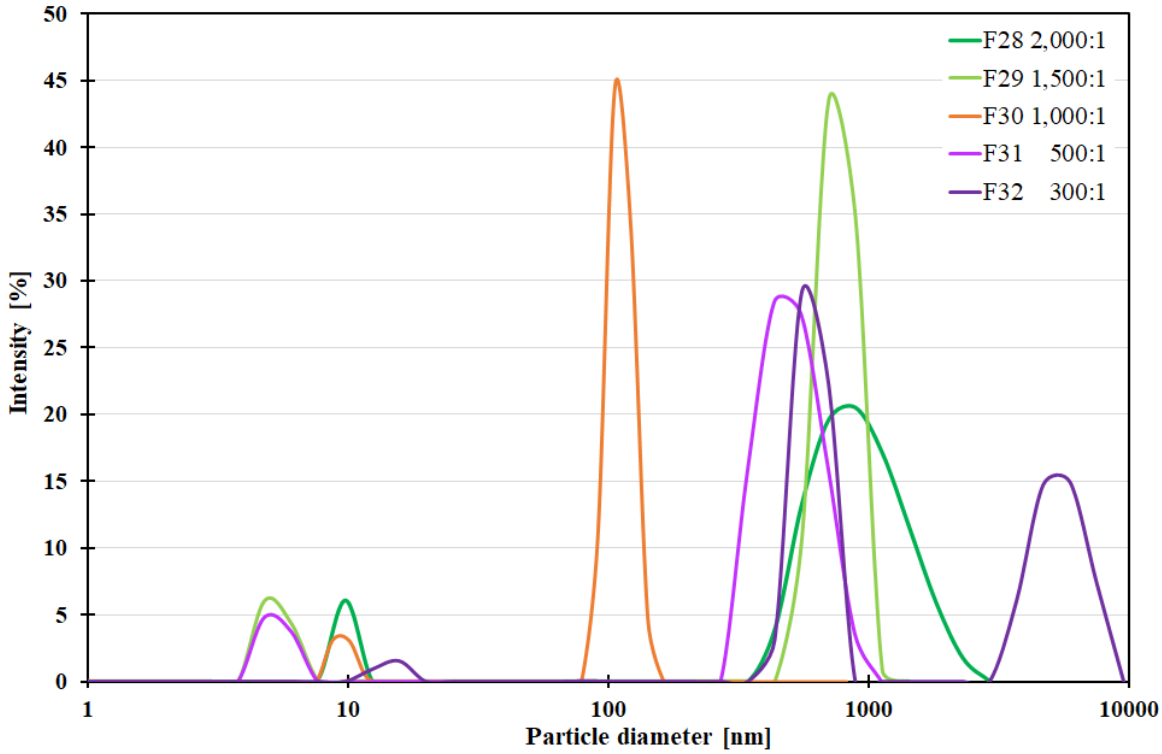

Figure 26 Particle size distribution and diameters of FGF2-LIP with different PC/FGF2 ratios

5.4.3 Encapsulation efficiency

The desired encapsulation efficiency was to be around 60 % and therefore a calibration for FGF2-STAB® concentration within the range of 10–100 µg/ml was used (4.4.3).

The resulting encapsulation efficiency did not fulfil the expectations of encapsulating 60 % or dosed FGF2-STAB®. The highest encapsulation efficiency was reached by using the ratio of PC/FGF2-STAB® 1,000:1 with the concentration of FGF2-STAB® in the formula 81.5 µg/ml, where it has reached 15 %. Efficiency of 12 % was reached when a ratio of 2,000:1 PC/FGF2-STAB® was used. Higher concentrations of loaded FGF2-STAB® did not result in higher encapsulation efficiency and reached only 4 % with 500:1 PC/FGF2-STAB® ratio and 7 % with 300:1 PC/FGF2-STAB® ratio.

An overview of the measured parameters of formulas *F28–31* regarding measured zeta potential [mV], concentration of FGF2-STAB® in each formula [µg/ml], liposome diameter [nm] and encapsulation efficiency [%] is shown in Figure 27 on the following page.

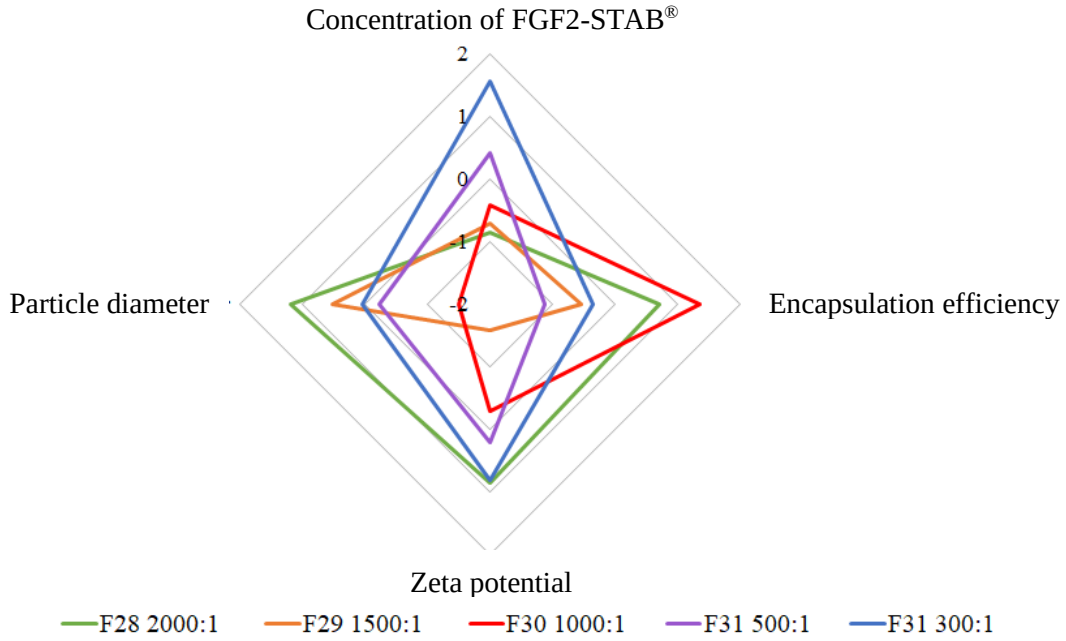

Figure 27 Comparison of F28–31 based on measured parameters; data standardized

5.4.4 Morphology of liposomes

To compare the morphology of empty liposomes (LIP) and FGF2-STAB® loaded liposomes (FGF2-LIP), formulas *F23* and *F30* were compared. Each contained 168 mg of PC, 40.8 mg CHOL, *F23* contained 100 µl of PBS, and *F30* contained 163 µl of FGF2-STAB® with concentration 1 mg/ml. *F23* is referred as LIP and *F30* is referred as FGF2-LIP.

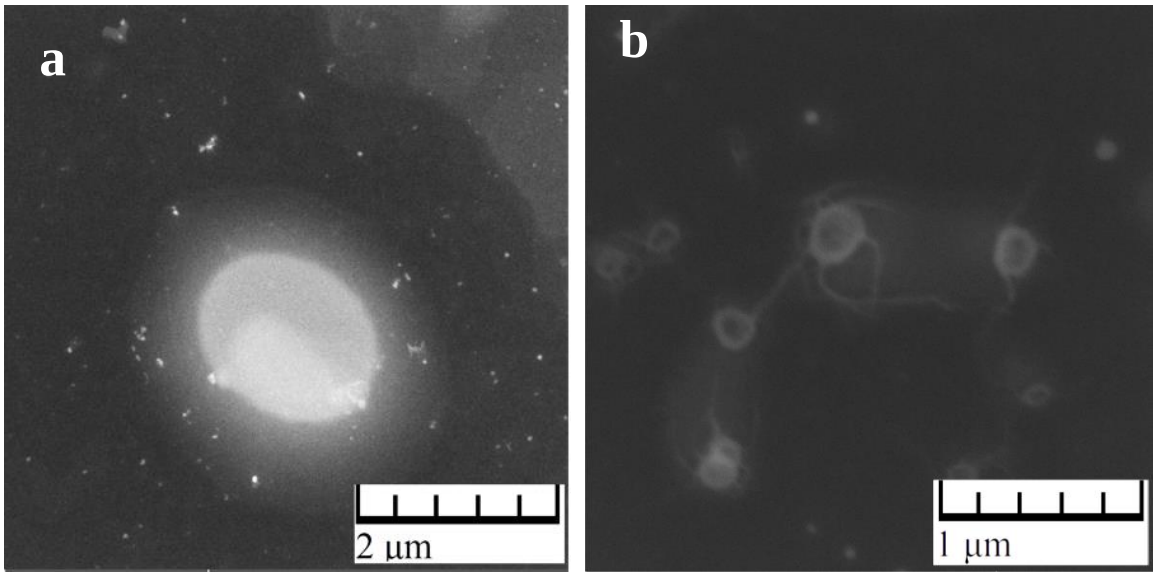

Figure 28 STEM images in transmission mode and dark field of LIP (a) and FGF2-LIP (b); samples were recorded at 50× (a) and 170× magnification (b)

As shown in Figure 28, LIP containing PBS gives much brighter contrast between the inside of the liposome, the liposome shell, and the outside of the liposome. This is due to the fact that the PBS contained in LIP has a much larger density than the FGF2-STAB® regarding the proton number. Recorded liposome in LIP was also much larger than liposomes in FGF2-LIP, which had a diameter around 2 μm, whereas most of the captured liposomes in FGF2-LIP had diameters around 200 nm. Imaged samples did not contain larger particles regarding DLS measurement results, but some were detected by STEM imaging. A difference in the thickness of the liposome shell is also noticeable. Liposomes in Figure 28 were not perfect spheres but possessed a rather an oval shape. In Figure 28 (b) and in the following Figure 29, small and thin lines coming from and through the liposome shells were detected. This could mean that some of the FGF2-STAB® in the formula attached and interacted with the shell of the liposomes rather than getting encapsulated inside of the liposome. FGF2-LIP also contained larger particles as displayed in Figure 29.

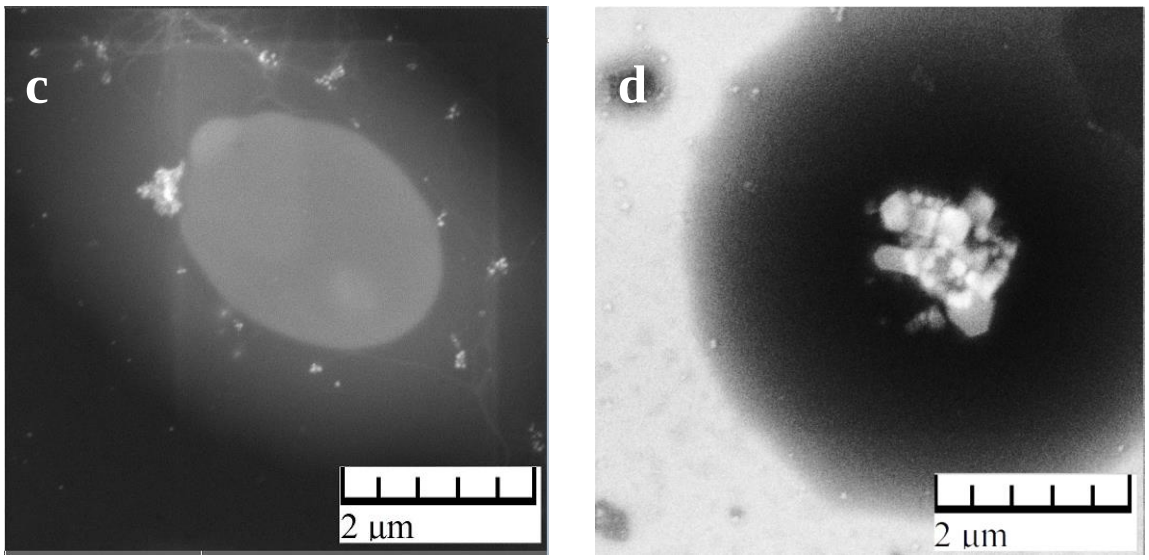

Figure 29 STEM images of FGF2-LIP at 100× magnification; images were taken in transmission mode dark field (c) and using an In-Beam secondary electron detector (d)

As seen in Figure 29 *(c)*, the imaged large liposome was formed by the inclusion of smaller liposomes into one larger liposome. This supports the theory that the prepared FGF2-STAB® encapsulated liposomes tend to agglomerate even though the overall measured particle size was around 100 nm. What is interesting in Figure 29 *(c)* and *(d)* is that the ions contained in PBS used for rehydration of the lipid film during sample preparation tend to agglomerate as well and form small crystals on top of the formed liposomes. This is clearly due to the storage time of seven days between the preparation and imaging of the samples. Yet this indicates that the liposome solution is saturated enough with salt ions from added PBS to form crystals.

Following, Figure 3*0 (e)* shows that even in FGF2-LIP sample, the majority of prepared liposomes were loaded with PBS, which corresponds to a measured encapsulation efficiency of 15 % in *F30*. *Figure 30* shows the aggregates *(e)* and agglomerates *(f)* of PBS loaded LIP formed within FGF2-LIP sample. This supports the theory of liposome agglomeration discussed in 5.1.2. What is interesting is that FGF2-LIP in this particular formula does not tend to agglomerate as much as PBS loaded LIP do.

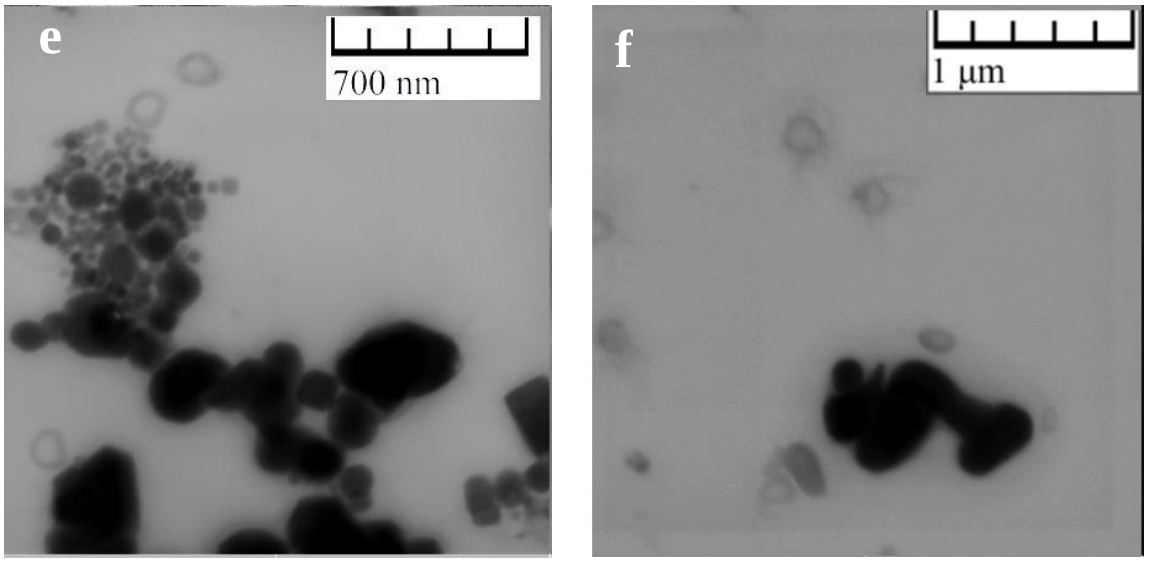

Figure 30 STEM images of FGF2-LIP at 150× magnification (e) and 100× magnification (f); images were taken in transmission mode and bright field

Since most of the aggregates were formed by PBS loaded liposomes, the density of these agglomerates is much larger than that of eventual agglomerates of FGF2-LIP due to the presence of inorganic substances in PBS. This also explains to a certain degree why the intensity of scattered light in DLS measurements was smaller in larger particles than in smaller particles. Larger particles were formed by aggregated smaller particles containing large amounts of inorganic PBS, the decrease in detected intensity could be possibly caused by absorption of the incident laser beam by the inorganic particles in the sample, since inorganic substances tend to absorb incident light more than organic substances.

Following Figure 31 confirms that agglomeration of prepared FGF2-LIP occurred by simple connection *(g)* as well as due to the inclusion of liposomes *(h)*.

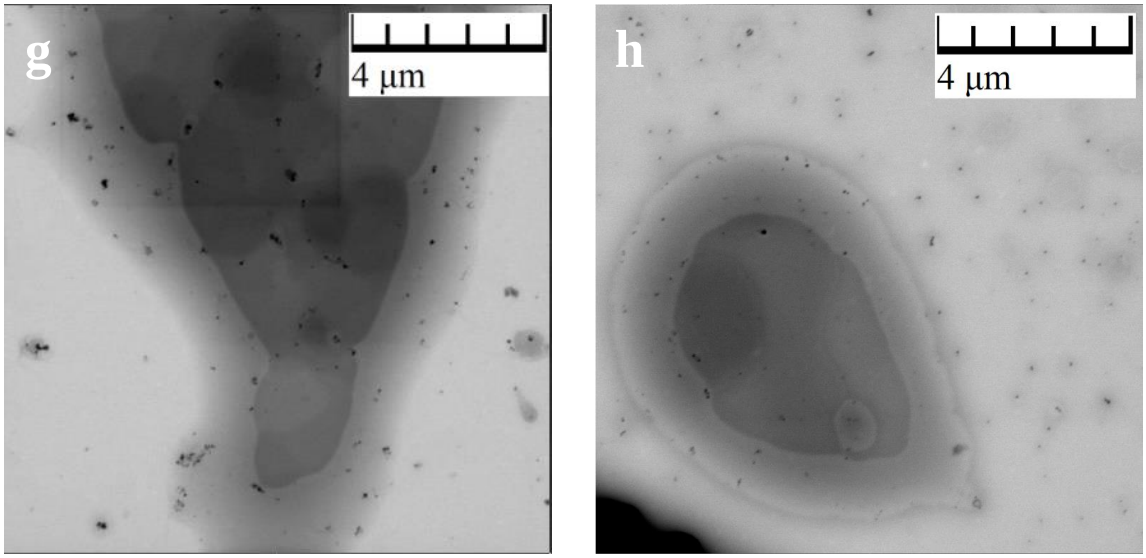

Figure 31 STEM images of FGF2-LIP at 25× magnification; images were taken in transmission mode and bright field

6 CONCLUSION

In the presented work liposomes composed of phosphatidylcholine and cholesterol were prepared using the phase evaporation technique. Stability of the prepared liposomes was determined via zeta potential, particle size distribution, and liposome size via dynamic light scattering and the morphology of liposomes was observed using scanning transmission electron microscopy. In liposomes containing FGF2-STAB®, the encapsulation efficiency was determined using UV-VIS spectrophotometer in the presence of Bradford reagent.

Liposome preparation technique was optimized first using only PBS as the solution to be encapsulated. Liposomes formed with the PC/CHOL ratio 10:1 containing a volume of PBS between 20–200 μl of PBS were prepared first. Liposomes containing 90.8 mg of PC and 9.0 mg of CHOL gave diameters and PSD curves considerable for transdermal delivery, but their zeta potentials were not decided as stable. Furthermore, liposomes containing 100 mg of PC and 10 mg of CHOL were prepared. These liposomes also did not give zeta potentials within the stable particle range and even though their diameters and PSD curves were favourable for transdermal delivery, these liposomes could not be considered as acceptable. Extrusion of these liposomes through 100 and 200 nm resulted in widening of the PSD curves, the shift of particles to larger diameters, and the intensity of the detected DLS signal decreased, probably due to the smaller particle aggregation and further agglomeration and due to absorption of incident light by inorganic particles present in PBS solution.

Later, a larger quantity of phosphatidylcholine was used to increase the stability of the system and to decrease the zeta potential of prepared liposomes to 150 and 163 mg. Dependency of measured variables was observed regarding PC/CHOL ratio being 4:1, 6:1, 8:1, and 10:1. It was determined that relatively good results gave liposomes formed with 163 mg of CHOL and 4:1 PC/CHOL ratio, where the zeta potential was relatively small, the liposome diameter was acceptable for transdermal delivery and its PSD curves were narrow and with high intensity of detected scattered light even after extrusion through polycarbonate membrane with pore size 200 and 100 nm.

It was discovered that the dependency of pH of liposome environment greatly affects its zeta potential and thus also stability. Samples contained 163 mg of PC and their PC/CHOL ratio were 4:1, 6:1, 8:1 and 10:1. Each of the prepared samples did not give zeta potential out of the range of ± 30 mV in the environment with pH 7 or pH 8. It was discovered that only liposomes with PC/CHOL ratio 10:1 reached stable zeta potential values at pH 11 and higher. Therefore, the prepared liposomes are not suitable for transdermal delivery due to the fact that they are not stable in the physiological pH range and some gain stability at pH that is unacceptable for working with proteins. This is probably related to the purity of PC being only 60 %. Other components present in phosphatidylcholine and the impurities probably cause the instability of the prepared liposomes.

FGF2-STAB® were prepared by using 163 mg of PC and 4:1 PC/CHOL ratio and different PC/FGF2-STAB® ratios from 300:1 up to 2,000:1. Regarding the zeta potential measurements, the smallest zeta potential was obtained by 1,500:1 PC/FGF2-STAB® ratio, but regarding the liposome size and PSD curves the best results were given by

the 1,000:1 PC/FGF2-STAB® ratio where the liposome diameter was 104.7 nm. This ratio also gave the largest encapsulation efficiency of all of the prepared ratios, staking at 14.9 %. The smallest encapsulation efficiency was given by 500:1 PC/FGF2-STAB® ratio staking at only 3.8 %.

Morphology of liposomes containing only PBS and containing also FG2-STAB® was observed using STEM. It was proved that the prepared liposomes form aggregates and agglomerates but that there is a major difference in liposomes containing FGF2-STAB® and only PBS. Liposomes containing only PBS tend to aggregate and agglomerate in a much higher rate that liposomes with FGF2-STAB® by simple adhesion of single liposomes and by inclusion of smaller liposomes into larger liposomes. It was also discovered that PBS present in samples containing FGF2-STAB® affects the morphology of the liposomes and probably due to fluctuations of ions present in PBS and results in the formation of small crystals on top of the liposome spheres.

In conclusion, the FGF2-STAB® encapsulation was successful but only to a certain level. The encapsulation efficiency of the prepared liposomes was far below the expectation of reaching the efficiency around 60 % (the prepared liposomes gave only around 15 %). Even though the liposome diameters and size distribution were satisfactory, its zeta potential was not. This was discovered to be due to the effect of pH of the environment. However, this work embodies the yet undiscovered potential of encapsulating FGF2-STAB® into liposomes. Since the liposome stability depends on pH, liposomes can be custom made for certain applications, where the pH is lower than the physiological pH 7. If the right phosphatidylcholine purity is used and the effect of potassium and sodium ions in PBS is tested, liposomes with great properties could be made in the laboratory.

REFERENCES

[1] BENSON, Heather A.E. and Sarika NAMJOSHI. 2008. Proteins and Peptides: Strategies for Delivery to and Across the Skin. *Journal of Pharmaceutical Sciences*. 97(9), 3591-3610.

[2] PIERRE, Maria Bernadete Riemma and Irina DOS SANTOS MIRANDA COSTA. 2011. Liposomal systems as drug delivery vehicles for dermal and transdermal applications. *Archives of Dermatological Research*. 303(9).

[3] HASAN, Mahadi., A. KHATUN, T. FUKUTA, et al., 2020. Noninvasive transdermal delivery of liposomes by weak electric current. *Advanced Drug Delivery Reviews*,

[4] JIJIE, Roxana, Alexandre BARRAS, Rabah BOUKHERROUB and Sabine SZUNERITS. 2017. Nanomaterials for transdermal drug delivery: beyond the state of the art of liposomal structures. *Journal of Materials Chemistry* B. 5(44), 8653-8675.

[5] PALASTANGA, N., FIELD, D., & SOAMES, R. (1989). *Anatomy and human movement: structure and function*. Oxford [England], Heinemann Medical Books

[6] KARP, G. *Cell and Molecular Biology: Concepts and Experiments*, 4th ed.; John Wiley & Son: Hoboken, NJ, 2006.

[7] ALBERTS, Bruce, Karen HOPKIN, Alexander JOHNSON, David O. MORGAN, Martin C. RAFF, Keith ROBERTS and Peter WALTER. [2019]. *Essential cell biology*. Fifth edition. New York.

[8] HERWADKAR, Anushree and Ajay K. BANGA. 2011. Transdermal Delivery of Peptides and Proteins. *Peptide and Protein Delivery*. Elsevier, 69-86.

[9] BENSON, Heather A.E. 2005. Transdermal Drug Delivery: Penetration Enhancement Techniques. *Current Drug Delivery*. 2(1), 23-33.

[10] FINNIN, Barrie C. and Timothy M. MORGAN. 1999. Transdermal penetration enhancers: Applications, limitations, and potential. *Journal of Pharmaceutical Sciences*. **88**(10), 955-958.

[11] HALL, John E. and Michael E. HALL. 2020. *Guyton and Hall Textbook of Medical Physiology*. 14th Edition. Jackson, Mississippi: Elsevier, 1152 p.

[12] LIU, Meifeng, Zehao LI, Huijuan WANG and Song DU. 2016. Increased cutaneous wound healing effect of biodegradable liposomes containing madecassoside: preparation optimization, in vitro dermal permeation, and in vivo bioevaluation. *International Journal of Nanomedicine*. 11, 2995-3007.

[13] NASR, Maha, Riham I. EL-GOGARY, Hend ABD-ALLAH and Mona ABDEL-MOTTALEB. 2020. Nanoparticulate systems for wound healing. *Nanopharmaceuticals*. Elsevier, 73-90.

[14] PALMER, Brian and Lisa DELOUISE. 2016. Nanoparticle-Enabled Transdermal Drug Delivery Systems for Enhanced Dose Control and Tissue Targeting. *Molecules*. 21(12).

[15] HARADA, Kayo., Teruo. MURAKAMI, Noboru. YATA and Shoso. YAMAMOTO. 1992. Role of Intercellular Lipids in Stratum Corneum in the Percutaneous Permeation of Drugs. *Journal of Investigative Dermatology*. **99**(3), 278-282.

[16] BENSON, Heather A. E. 2011. Skin Structure, Function, and Permeation. *Topical and Transdermal Drug Delivery*. Hoboken, USA, 1-22.

[17] SILER-MARINKOVIC, Slavica. 2016. Liposomes as Drug Delivery Systems in Dermal and Transdermal Drug Delivery. *Percutaneous Penetration Enhancers Chemical Methods in Penetration Enhancement*. Berlin, Heidelberg: Springer Berlin Heidelberg, pages 15-38.
[18] ZHANG, Hongwei. 2017. Thin-Film Hydration Followed by Extrusion Method for Liposome Preparation. *Liposomes*. New York, NY: Springer New York, 17-22. Methods in Molecular Biology.
[19] LÓPEZ-PINTO, J.M., M.L. GONZÁLEZ-RODRÍGUEZ and A.M. RABASCO. 2005. Effect of cholesterol and ethanol on dermal delivery from DPPC liposomes. *International Journal of Pharmaceutics.* 298(1), 1-12.
[20] LEE, Kuen Yong and Soon Hong YUK. 2007. Polymeric protein delivery systems. *Progress in Polymer Science*. 32(7), 669-697.
[21] BAREL, A. O., Marc PAYE and Howard I. MAIBACH. 2014. *Handbook of cosmetic science and technology*. Fourth edition. Boca Raton.
[22] AKBARZADEH, Abolfazl, Rogaie REZAEI-SADABADY, Soodabeh DAVARAN, et al. 2013. Liposome: classification, preparation, and applications. *Nanoscale Research Letters*. **8**(1).
[23] SHARMA, A. 1997. Liposomes in drug delivery: Progress and limitations. *International Journal of Pharmaceutics*. 154(2), 123-140.
[24] LOU, Gustavo, Giulia ANDERLUZZI and Stuart WOODS. 2019. A novel microfluidic-based approach to formulate size-tuneable large unilamellar cationic liposomes: Formulation, cellular uptake and biodistribution investigations. *European Journal of Pharmaceutics and Biopharmaceutics.* 143, 51-60.
[25] IBARAKI, Hisako, Takanori KANAZAWA, Chihiro OOGI, Yuuki TAKASHIMA and Yasuo SETA. 2019. Effects of surface charge and flexibility of liposomes on dermal drug delivery. *Journal of Drug Delivery Science and Technology*. **50**, 155-162.
[26] PROW, Tarl W., Jeffrey E. GRICE, Lynlee L. LIN, et al. 2011. Nanoparticles and microparticles for skin drug delivery. *Advanced Drug Delivery Reviews*. 63(6), 470-491.
[27] MBAH, Chukwuemeka C, Philip F BUILDERS and Anthony A. ATTAMA. 2013. Nanovesicular carriers as alternative drug delivery systems: ethosomes in focus. *Expert Opinion on Drug Delivery*. **11**(1), 45-59.
[28] KUMAR, Lalit, Shivani VERMA, Kuljit SINGH, Deo Nandan PRASAD and Amit Kumar JAIN. 2016. Ethanol Based Vesicular Carriers in Transdermal Drug Delivery: Nanoethosomes and Transethosomes in Focus. *NanoWorld Journal.* **2**(3).
[29] KUMAR, Raman and Sandeep KUMAR. 2020. ETHOSOMES: The Promising Carriers for the Transdermal Delivery of Drugs. *Journal Of Pharmacy And Biological Sciences*. 15(4), 11–17
[30] FU, Xianglei, Yanbin SHI, Hui WANG, Xiaogang ZHAO, Qifeng SUN, Yi HUANG, Tongtong QI and Guimei LIN. 2019. Ethosomal Gel for Improving Transdermal Delivery of Thymosin β-4. *International Journal of Nanomedicine*. 14, 9275-9284.
[31] Shajan Abraham et al. 2019. A review on ethosomes: novel drug delivery system. *Journal of Global Trends Pharm Sci*. 10(3), 6340–6346

[32] TOSATO, Maira Gaspar, Julie V. MAYA GIRÓN, Airton A. MARTIN, Vamshi KRISHNA TIPPAVAJHALA, Mónica FERNÁNDEZ LORENZO DE MELE and Lelia DICELIO. 2018. Comparative study of transdermal drug delivery systems of resveratrol: High efficiency of deformable liposomes. *Materials Science and Engineering:* C. **90**, 356-364.
[33] NAINWAL, Nidhi, Sunil JAWLA, Ranjit SINGH and Vikas Anand SAHARAN. 2018. Transdermal applications of ethosomes – a detailed review. *Journal of Liposome Research*. 29(2), 103-113.
[34] ANOOP, K. R. 2012. Ethosomes for transdermal and topical drug delivery. *International Journal of Pharmacy and Pharmaceutical Sciences*. 4(3), 17–24.
[35] Singh Satnam and Kumar Sandeep. 2018.Ethosomes: A New Pathway for Novel Drug Delivery., *Indo American Journal of Pharmaceutical Sciences*, 05(08)
[36] Divya Aggarwal et al. 2016. Ethosomes: A review. *International Journal of Pharmaceutical and Medicinal Research*. 4(4), 354-363
[37] GARG, Varun, Harmanpreet SINGH, Sneha BIMBRAWH, Sachin Kumar SINGH, Monica GULATI, Yogyata VAIDYA and Prabhjot KAUR. 2017. Ethosomes and Transfersomes: Principles, Perspectives and Practices. *Current Drug Delivery*. 14(5).
[38] FERNÁNDEZ-GARCÍA, Raquel, Aikaterini LALATSA, Larry STATTS, Francisco BOLÁS-FERNÁNDEZ, M. Paloma BALLESTEROS and Dolores R. SERRANO. 2020. Transferosomes as nanocarriers for drugs across the skin: Quality by design from lab to industrial scale. *International Journal of Pharmaceutics.* **573**.
[39] GILLET, A., F. LECOMTE, P. HUBERT, E. DUCAT, B. EVRARD and G. PIEL. 2011. Skin penetration behaviour of liposomes as a function of their composition. *European Journal of Pharmaceutics and Biopharmaceutics*. **79**(1), 43-53.
[40] G. Cevc, G. Blume, Lipid vesicles penetrate into intact skin owing to the transdermal osmotic gradients and hydration force, *Biochim. Biophys*. Acta. 1104 (1992) 226–232.
[41] SOLANKI *et al.* (2016). Transferosomes – A review. *World Journal of Pharmacy and Pharmaceutical Sciences.* 5(10), 435–449
[42] MUZZALUPO, Rita and Elisabetta MAZZOTTA. 2019. Do niosomes have a place in the field of drug delivery? *Expert Opinion on Drug Delivery*. **16**(11), 1145-1147.
[43] GUPTA, Prem N., Vivek MISHRA, Amit RAWAT, Praveen DUBEY, Sunil MAHOR, Sanyog JAIN, D.P. CHATTERJI and Suresh P. VYAS. 2005. Non-invasive vaccine delivery in transfersomes, niosomes and liposomes: a comparative study. *International Journal of Pharmaceutics*. **293**(1-2), 73-82.
[44] GE, Xuemei, Minyan WEI, Suna HE and Wei-En YUAN. 2019. Advances of Non-Ionic Surfactant Vesicles (Niosomes) and Their Application in Drug Delivery. *Pharmaceutics*. **11**(2).
[45] MANCONI, Maria, Chiara SINICO, Donatella VALENTI, Giuseppe LOY and Anna M FADDA. 2002. Niosomes as carriers for tretinoin. I. Preparation and properties. *International Journal of Pharmaceutics*. **234**(1-2), 237-248.
[46] MORE, Vrunal V., Ritu M. GILHOTRA, Manoj M. NITALIKAR and Prajakta K. KHULE. 2018. Niosome: Comprehensive review. *Asian Journal of Pharmaceutics.* **12**(4), 1159–1164.

[47] RAJERA, Rampal, Kalpana NAGPAL, Shailendra Kumar SINGH and Dina Nath MISHRA. 2011. Niosomes: A Controlled and Novel Drug Delivery System. *Biological and Pharmaceutical Bulletin*. **34**(7), 945-953.
[48] Dhand R. (2004). New frontiers in aerosol delivery during mechanical ventilation. *Respiratory Care* 49(6), 666–677
[49] ISHIDA, Tatsuhiro, Hideyoshi HARASHIMA and Hiroshi KIWADA. 2002. Liposome Clearance. *Bioscience Reports*. **22**(2), 197-224.
[50] WANG, Guijun. 2016. Liposomes as Drug Delivery Vehicles. *Drug Delivery*. Hoboken, NJ, USA, 272-298.
[51] LANÍKOVÁ, P. *Studium vlivu liposomálních platinových 56rotein56ic na nádorové buňky pomocí voltametrických metod.* Brno: Vysoké učení technické v Brně, Fakulta elektrotechniky a komunikačních technologií, 2017. 83 s. Vedoucí diplomové práce Ing. Et Ing. David Hynek, Ph.D.
[52] ANWEKAR, H. (2011). Liposome as drug carriers. *International Journal of Pharmacy and Life Sciences*. 2(7), 945–951
[53] REZAEI, Nastaran, Faramarz MEHRNEJAD, Zahra VAEZI, Mosslim SEDGHI, S. Mohsen ASGHARI and Hossein NADERI-MANESH. 2020. Encapsulation of an endostatin peptide in liposomes: Stability, release, a nd cytotoxicity study. *Colloids and Surfaces B: Biointerfaces.* 185.
[54] SWAMINATHAN, Janani and Carsten EHRHARDT. 2012. Liposomal delivery of proteins and peptides. *Expert Opinion on Drug Delivery*. **9**(12), 1489-1503.
[55] WEINER, Alan L. 1994. Liposomes for Protein Delivery: Selecting Manufacture and Development Processes. *Immuno Methods*. **4**(3), 201-209.
[56] EDELMAN, Elazer R., Edith MATHIOWITZ, Robert LANGER and Michael KLAGSBRUN. 1991. Controlled and modulated release of basic fibroblast growth factor. *Biomaterials*. 12(7), 619-626.
[57] BEENKEN, Andrew and Moosa MOHAMMADI. 2009. The FGF family: biology, pathophysiology and therapy. *Nature Reviews Drug Discovery*. 8(3), 235-253.
[58] BIKFALVI, Andreas, Sharon KLEIN, Giuseppe PINTUCCI and Daniel B. RIFKIN. 1997. Biological Roles of Fibroblast Growth Factor-2*. *Endocrine Reviews*. 18(1), 26-45.
[59] NUGENT, Matthew A and Renato V IOZZO. 2000. *Fibroblast growth factor-2*. 32(2), 115-120.
[60] Faham, S., Hileman, R. E., Fromm, J. R., Linhardt, R. J., & Rees, D. C. (1996). Heparin Structure and Interactions with Basic Fibroblast Growth Factor. *Science*, 271(5252), 1116–1120.
[61] OKADA-BAN, Mai, Jean Paul THIERY and Jacqueline JOUANNEAU. 2000. *Fibroblast growth factor-2*. 32(3), 263-267.
[62] SIMONATO, M. and S. ZUCCHINI. 2009. NEUROTROPHIC FACTORS | Fibroblast Growth Factor-2. *Encyclopedia of Basic Epilepsy Research*. Elsevier, 916-921.
[63] Iozzo RV, editor. *Proteoglycans: structure, biology, and molecular interactions*. New York: Marcel Dekker, Inc.; 2000
[64] VOET, Donald and Judith G. VOET. 2011. *Biochemistry*. 4th ed. Hoboken: Wiley.
[65] DVORAK, Pavel, David BEDNAR, Pavel VANACEK, et al. 2018. Computer - assisted engineering of hyperstable fibroblast growth factor 2. *Biotechnology and Bioengineering*. **115**(4), 850-862.

[66] LOTZ, Steven, Susan GODERIE, Nicolas TOKAS, et al. 2013. Sustained Levels of FGF2 Maintain Undifferentiated Stem Cell Cultures with Biweekly Feeding. *PLOS ONE*. 8(2).
[67] CALLAGHAN, Matthew J., Edward I. CHANG, Natalie SEISER, Shahram AARABI, Shadi GHALI, Elspeth R. KINNUCAN, Bruce J. SIMON and Geoffrey C. GURTNER. 2008. Pulsed Electromagnetic Fields Accelerate Normal and Diabetic Wound Healing by Increasing Endogenous FGF-2 Release. *Plastic and Reconstructive Surgery*. 121(1), 130-141.
[68] FEI, Yurong, Gloria GRONOWICZ and Marja M. HURLEY. 2013. Fibroblast Growth Factor-2, Bone Homeostasis and Fracture Repair. *Current Pharmaceutical Design*. 19(19), 3354-3363.
[69] YANG, Wenyu, Yiting CAO, Zhe ZHANG, Fuchong DU, Yanping SHI, Xuemin LI and Qiqing ZHANG. 2018. Targeted delivery of FGF2 to subchondral bone enhanced the repair of articular cartilage defect. *Acta Biomaterialia*. 69, 170-182.
[70] NAGAYASU-TANAKA, Toshie, Jun ANZAI, Shu TAKAKI, et al. 2015. Action Mechanism of Fibroblast Growth Factor-2 (FGF-2) in the Promotion of Periodontal Regeneration in Beagle Dogs. *PLOS ONE*. 10(6).
[71] ONO, Ichiro. 2011. A study on the alterations in skin viscoelasticity before and after an intradermal administration of growth factor. *Journal of Cutaneous and Aesthetic Surgery.* 4(2).
[72] ONO, Ichiro, Yoshikiyo AKASAKA, Risa KIKUCHI, Akiko SAKEMOTO, Takafumi KAMIYA, Toshiharu YAMASHITA and Kowichi JIMBOW. 2007. Basic fibroblast growth factor reduces scar formation in acute incisional wounds. *Wound Repair and Regeneration.* 15(5), 617-623.
[73] LIN, Wei-hong, Li-Jun XIANG, Hong-Xue SHI, et al. 2015. Fibroblast Growth Factors Stimulate Hair Growth through β -Catenin and Shh Expression in C57BL/6 Mice. *BioMed Research International*. 2015, 1-9.
[74] SHE, Zhen, Chunxia WANG, Jun LI, Gleb B. SUKHORUKOV and Maria N. ANTIPINA. 2012. Encapsulation of Basic Fibroblast Growth Factor by Polyelectrolyte Multilayer Microcapsules and Its Controlled Release for Enhancing Cell Proliferation. *Biomacromolecules*. 13(7), 2174-2180.
[75] Y. Akasaka, I. Ono, T. Kamiya, *et al.*, The Mechanisms Underlying Fibroblast Apoptosis Regulated by Growth Factors during Wound Healing, *Journal of Pathology*, Vol. 221, No. 3, 2010, pp. 285-299.
[76] OKABE, Keisuke, Ruka HAYASHI, Noriko ARAMAKI-HATTORI, Yoshiaki SAKAMOTO and Kazuo KISHI. 2013. Wound Treatment Using Growth Factors. *Modern Plastic Surgery*. **03**(03), 108-112.
[77] XU, He-Lin, Pian-Pian CHEN, De-Li ZHUGE, Qun-Yan ZHU, Bing-Hui JIN, Bi-Xin SHEN, Jian XIAO and Ying-Zheng ZHAO. 2017. Liposomes with Silk Fibroin Hydrogel Core to Stabilize bFGF and Promote the Wound Healing of Mice with Deep Second-Degree Scald. *Advanced Healthcare Materials.* **6**(19).
[78] LYSÁKOVÁ, Klára. 2019. *Optimalizace metod pro analýzu proteinů uvolněných z termocitlivého hydrogelu.* Brno. Diplomová práce. Vysoké učení technické v Brně. Vedoucí práce Doc. Ing. Lucy Vojtová, Ph.D.
[79] XIANG, Qi, Jian XIAO, Hongbo ZHANG, et al. 2011. Preparation and characterisation of bFGF-encapsulated liposomes and evaluation of wound-healing activities in the rat. *Burns.* 37(5), 886-895.

[80] XU, He-Lin, Pian-Pian CHEN, Li-fen WANG, Wei XUE and Ting-Ling FU. 2018. Hair regenerative effect of silk fibroin hydrogel with incorporation of FGF-2-liposome and its potential mechanism in mice with testosterone-induced alopecia areata. *Journal of Drug Delivery Science and Technology.* **48**, 128-136.
[81] LAOUINI, A., C. JAAFAR-MAALEJ, I. LIMAYEM-BLOUZA, S. SFAR, C. CHARCOSSET and H. FESSI. 2012. Preparation, Characterization and Applications of Liposomes: State of the Art. *Journal of Colloid Science and Biotechnology*. 1(2), 147-168.
[82] JULIANO, R.L. and D. STAMP. 1975. The effect of particle size and charge on the clearance rates of liposomes and liposome encapsulated drugs. *Biochemical and Biophysical Research Communications*. 63(3), 651-658.
[83] Qi L, Xu Z, Jiang X, et al. Cytotoxic activities of chitosan nanoparticles and copper-loaded nanoparticles. *Bioorg Med Chem Lett* 2005; 15:1397–9.
[84] LOMBARDO, Domenico, Pietro CALANDRA, Maria TERESA CACCAMO, Salvatore MAGAZÙ and Mikhail ALEKSEYEVICH KISELEV. 2019. Colloidal stability of liposomes. *AIMS Materials Science.* 6(2), 200-213
[85] ARTS, T.J.C., J. LAVEN, F. VAN VOORST VADER and Th. KWAAITAAL. 1994. Zeta potentials of tristearoylglycerol crystals in olive oil. Colloids and Surfaces. *Physicochemical and Engineering Aspects.* 85(2-3), 149-158.

LIST OF ABREVIATIONS

FGF2-STAB®	fibroblast growth factor-2 hyper stabilized
PC	phosphatidylcholine
DLS	dynamic light scattering
STEM	scanning transmission electron microscopy
UV-VIS spectrophotometer	ultraviolet-visible spectrophotometer
UV	ultraviolet-visible
SC	stratum corneum
ECM	extracellular matrix
T_M	phase transition temperature
PEG	polyethylene glycol
ULV	unilamellar vesicles
SUV	small unilamellar vesicles
LUV	large unilamellar vesicles
GUV	giant unilamellar vesicles
MLV	multilamellar vesicles
DNA	deoxyribonucleic acid
RNA	ribonucleic acid
TEM	transmission electron microscopy
bFGF	basic fibroblast growth factor
mRNA	messenger RNA
FGFRs	fibroblast growth factor receptors
HS	heparan sulfate
KH_2PO_4	potassium phosphate monobasic
K_2HPO_4	potassium phosphate dibasic
NaCl	sodium chloride
H_3PO_4	phosphoric acid
KOH	potassium hydroxide
PBS	phosphate buffer saline
w/o emulsion	water in oil emulsion
rpm	rounds per minute
CHOL	cholesterol
ZP	zeta potential
PSD	particle size distribution